FINITE ELEMENT MODELLING OF GUIDED WAVES IN TUBES FOR INSPECTION OF CRACKS

by

CH. RAMA KANTH

DEPARTMENT OF MECHANICAL ENGINEERING

INDIAN INSTITUTE OF TECHNOLOGY KANPUR

APRIL, 1998

FINITE ELEMENT MODELLING
OF
GUIDED WAVES IN TUBES
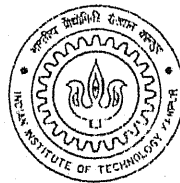## FOR
INSPECTION OF CRACKS

A Thesis Submitted

in Partial Fulfilment of the Requirements

for the Degree of

Master of Technology

by

CH.RAMA KANTH

to the

DEPARTMENT OF MECHANICAL ENGINEERING

INDIAN INSTITUTE OF TECHNOLOGY KANPUR

March, 1998
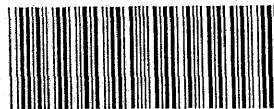
ME- 1998 - M - KAN - FIN
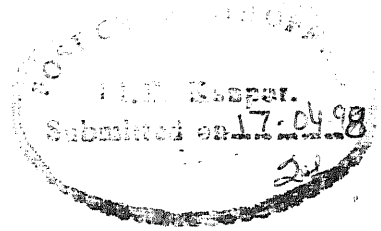
Entered in System

Nimisha
4-6-98

CERTIFICATE

It is certified that the work contained in the thesis entitled **FINITE ELEMENT MODELLING OF GUIDED WAVES IN TUBES FOR INSPECTION OF CRACKS** by **CH.RAMA KANTH**, has been carried out under my supervision and that this work has not been submitted elsewhere for a degree.

Dr. N.N.KISHORE
Professor
Department of Mechanical Engineering
Indian Institute of Technology Kanpur

March,1998

Dedicated to -

My beloved Mother & Babli

A C K N O W L E D G E D G E M E N T S

The author, with great pleasure expresses his gratitude to Dr. N.N.KISHORE, whose immense knowledge of the subject and practical experience in the field, with active participation guided me to reach a solution to the problem. It has been a great pleasure to work under his able guidance.

Particular thanks are due to Mr. S.K.Rathore, Mr.S.K.Singal, Mr.Ravi, Mr.A.K.Agarwal, Mr.B.Rameswar Reddy and all other friends for their help offered during the the course of work.

CH.RAMA KANTH
IIT Kanpur
March,1998.

SYNOPSIS

Ultrasonic means have been widely used in a variety of engineering applications for the nondestructive evaluation of pipes and tubes. Defects such as cracks and inclusions act as a source locations of wave scattering when illuminated by an incident ultrasonic pulse through reflection, diffraction and mode-conversion. Interaction of elastic wave with cracks provide all the necessary information regarding the inverse characterization of the defects which has not yet been thoroughly solved yet. The study of forward scattering problem or the determination of wave field scattered by defects would provide more knowledge in implementing the inverse algorithms. Analytical solution for the forward scattering is available only for particular scattering solutions.

There are several popular NDE methods that have their own advantages and disadvantages for the practical inspection work. Recently, Ultrasonic guided waves have been found to have some specific advantage in tubing inspection. The dominent benifit is the penetration ability to inspect the entire length of the tube so that the ultrasonic guided wave technique can quickly locate the defects in tubing without moving the ultrasonic transducer.

In the present work a finite element model has been developed to study the elastic wave propagation and scatering in thin tubes. Interaction of the guided wave with the cracks has been studied, with the basic aim of detecting the axial as well as the angular location of the crack.

From the results it is concluded that a combination of three source locations circumferentially located at an angle of 120 degrees aparts is very effective in scanning the entire surface of the tube. The loading in the tangential plane proved effective. Some guide lines are provided to locate the axial and circumferential position of the cracks.

• • •

Contents

List of Figures

Chapter 1

Introduction

1.1 Introduction

Understanding the propagation of waves through elastic media is of potential benefit in several fields of science and engineering. The effects of very short term impact loads on the structures can be understood fully if analyzed in terms of propagation of stress waves. Crack propagation or the interaction of dynamic stress waves with the existing cracks, voids or inclusions in a material can be predicted if the dynamic effects are taken into account. Further the knowledge of elastic wave propagation is essential in a host of other fields such as ultrasonics, geophysics, electronics etc.

Ultrasonics is a major field of application of wave phenomena. The interest here lies in the ultrasonic nondestructive evaluation of materials which is widely used in aerospace, transportation, chemical and energy industries for the detection and characterization of defects such as cracks and inclusions in critical structural members. Such tests are needed both in the manufacturing phases of the products in order to assure the quality as well as during their operating life time in order to prevent failure and asses the residual life.

In essence, ultrasonic guided wave inspection involves introducing a stress pulse into the material under inspection and observing the defects such as cracks and inclusions act as source locations of wave scattering when illuminated by an incident pulse through reflection, diffraction and mode-conversion. An adequate understanding of the wave propagation is essential for the optimization of the current NDT techniques and also for the development of the new techniques.

1.2 Literature Survey

Elastic wave propagation and scattering has been under investigation in many fields such as seismology, geophysics, electronics and applied mechanics for many years. An excellent review of the state of art of the theory of stress wave propagation and scattering was given by Pao[1].

The current developments in high speed computers, range of work stations and graphics packages are all bringing revolutionary changes in the numerical modeling of ultrasonic NDT. Examples of most modeling techniques employed to study ultrasonic NDT have been reported in the series "Review of progresses in quantitative NDE" [2] and various other publications[3,4,5].

1.2.1 Guided waves and NDT

There are several popular NDE methods, such as bulk wave ultrasonic, radiography acoustic emission, eddy currents and visual-optics, that have their own advantages and disadvantages for practical inspection work. Recently developed ultrasonic guided wave techniques have some benefits in tubing inspection.

Guided waves, are nothing but waves propogating through bodies with narrow cross sections. Plate, or Lamb waves which propagate in thin layers of materials are some examples. These waves, unlike bulk waves, excite the whole cross section of the thin structure and propagate in a specific direction. This specific advantage of the guided waves has lead to its use in NDT for defect classification and characterization.

The dominant benefit is the penetration ability to inspect an entire length of the tube so that the ultrasonic guided wave technique can quickly locate the defects in tubing without moving the ultrasonic guided wave transducer.

Guided wave propagation along the pipe provide a potentially very attractive inspection technique. They may be excited from the pipe outer wall and say, only a key hole in the insulation can be made to allow access for a transducer system. The waves can propagate tens of meters along the pipe, so a long length pipe may be inspected from each transducer position.

Many workers have investigated the use of guided waves for the inspection of plate like

structures and there has been a considerable amount of work on there use in the inspection of pipes and tubing[23-26].

The first general solution of harmonic wave propagation in an infinitely long elastic hollow cylinder was obtained by Gazis and his coworkers using elasticity theory[27-28]. Armenaks,Gazis and Herrmann summerized their work into a book entitled "Free Vibrations of Circular Cylindrical Shells" including numerical results of some ultrasonic guided wave modes[29]. Ultrasonic guided wave propagation in hollow cylinders was studied by Fitch[30]. For the generation of ultrasonic guided waves in heat exchanger tubing, Silk and Bainton[31] investigated piezoelectric ultrasonic probes to access the inside layer of the tube. Alleyne et al.[32] suggested the use of the fastest mode in a non-dispersive region of frequency range to minimize dispersion effects over long distances. For defect detection and optimization, Dirti et al.[33,34] discussed mode selection criterion based on the acoustic field across the thickness of the of the wave guide, explaining why certain modes are more sensitive to certain geometries of defects than others. Rose et al.[35,36,37] employed the mode control concept and reported experimental results for multiple crack detection, a water insensitive mode, and long range inspection. There is some research in defect characterization and sizing studies using ultrasonic guided wave technique in both experiment and theory[38,39]. Very little has been done for the analytical solution of the acoustic wave field in tubing for an applied non-axisymmetric loading. Dirti and Rose[40] published a paper which contained the normal mode expansion technique to obtain the acoustic field distribution along a tube for an arbitrary applied surface traction.

Alleyne et.al have worked on a project whose ultimate aim is to develop a guided wave testing technique for the inspection of pipe work in chemical plant, the target being to detect any areas of corrosion larger than 3Tx3T in area and T/2 deep where T is the pipe wall thickness. The technique is to work on a insulated pipe in the 2-12 inch nominal bore range and an inspection range of at least 15m from the transducer position is required.

A first concern on the use of ultrasonic guided waves in tubing is to find the useful modes. Theory of elasticity and basic wave mechanics can be used to predict the infinite number of modes that can be generated in a tube. The modes can be represented on dispersion curves for given frequency and phase velocity ranges. Also the group velocity dispersion curves can be used for an identification of received modes, mode selection, and defect location.

Guided wave field analysis or wave structure through the thickness of tubing is one of the important parameters in selecting modes for a certain purpose. It is shown in a paper by Pilarski, Ditri, and Rose[25] that points of dominant in plane displacement are achieved for a phase velocity close to the longitudinal wave velocity. Points in the neighbourhood of these special points have dominant in plane components but still some out of plane component which allows coupling and minimal leakage of energy to fluid loaded tubes from the outside if this situation are encountered. From a defect detection point of view, the displacement field analysis gives a good explanation of the sensitivity changes to defects. For long range screening purposes, it is better to use modes with less outside sensitivity or/and lower frequencies. Modes with power concentration on the surface are more sensitive to surface cracks than the modes with power concentration on the center line of the tube thickness.

Great progress is being made on the use of axisymmetric ultrasonic guided waves in tubing for defect detection, classification and sizing. Benefits of excellent penetration and sensitivity to certain defects are possible. However, ultrasonic guided wave propagation and reflection in tubing is still not completely understood. For more comprehensive knowledge of ultrasonic guided wave tubing, a study on non-axisymmetric modes cannot be avoided. A number of non-axisymmetric modes close to the axisymmetric modes on a dispersion diagram often makes it difficult to generate a single axisymmetric mode in tubing. Also, non-axisymmetric reflections occur due to non-nonaxisymmetric defects, even for axisymmetric impingment.

1.2.2   Use of Finite Element Method in Wave Propogation Analysis

The development of appropriate methods for the analysis of shell structures is increasingly demanded to ensure the integrity of structural designs. Analytical solutions to shell structures are limited in scope and in general are not applicable to arbitrary shapes, load conditions, irregular stiffening and support conditions, cutouts and many other aspects of practical design. The finite element method has consequently become prominent in the analysis of such shells in view of the ease with which such complexities can be dealt with.

Although finite element procedures have been applied to shell analysis for over twenty years, the search for suitable elements which are readily applicable to general shell struc-

tures is still in progress[6-9]. Three distinct approaches to the finite element representation of shell structures have been employed based on

(i) flat triangular or quadrilateral elements,

(ii) curved elements formulated on the basis of various shell theories and

(iii)   elements derived from three-dimensional elements by the use of the degeneration methods.

The first numerical studies of shell problems involved facetting the shell by plane triangular elements, onto which a membrane stiffness was superimposed . The results obtained were found to be satisfactory, but depending on the problem, very fine meshes had to be employed. A number of difficulties and shortcomings arise from the application of flat elements to curved shells[10], such as the presence of 'discontinuity' in bending moments, which do not appear in the continuously curved actual structures.

In the second approach a classical concept is employed, whereby a shell theory is used as the starting point of the finite element formulation. Different shell theories have been developed from the three dimensional field of equations by incorporating various assumptions appropriate to the structural behaviour. A variety of finite elements with different degrees of complexity have been formulated for deep and shallow shells. Curved shell elements based on the Kirchhoffs-Love theory guarantee a high solution accuracy but are complicated by convergence and compatibility requirements. In the case of a fully nonlinear analysis, additional difficulties arise in the formulation of efficient finite elements due to the unavalibility of a general nonlinear shell theory.

The third approach employed in the formulation of shell elements avoids the complexities of fully general shell theories by discretizing directly the three-dimensional equations of continuum mechanics. Isoparametric elements with independent rotational and displacement degrees of freedom(dof) are employed, in which the three dimensional stress and strain conditions are degenerated to shell behaviour. The procedure was originally introduced by Ahmad et al. [11] for the linear analysis of moderately thick shells. Although this type of element seemed to be very promising when it was introduced, difficulties later appeared, due to the degeneration process, as the thickness of the element was reduced. A great improvement of the model was achieved by means of the so-called reduced integration technique.

In numerical modeling applied to elastic waves much effort has been concentrated on the finite difference method and more recently, on the finite element method. These models consider mid-frequency scattering where complex mode-conversion phenomenon is encountered. Such models give a complete description of the time development of the wave-field of interest. They can also model mixed solid-fluid problems and can model a wide range of material properties.

Developments in the finite difference modeling of ultrasonic wave propagation were reported by Bond et al [15]. Results were obtained for a range of two dimensional geometries with pulsed plane wave excitation and found to agree with experiments. In addition immersion inspection systems were modeled where there is propagation in both an elastic solid and a viscous fluid. Finite difference model results were produced for pulsed wave scattering by a semi-infinite 2-D slit and compared with those obtained from GTD[16]. Bond & Saffari[17] has emphasized the mode-conversion technique in ultrasonic NDT and has given experimental results of crack detection by making use of the mode-conversion phenomenon.

The use of FEM to model ultrasonic scattering is rather resent. Its superiority lies in its ability to handle complex shaped domains and defect shapes, discontinuities, inhomogenities, nonlinearities in material etc. The pioneering effort in this direction has been by Lord [20,21] and his co-workers who produced a scheme which employ a finite element formulation for spatial discretization and finite difference scheme for temporal discretization. Ludwig and Lord [20] reported details of a 2-d finite element code employing Newmark's scheme for time integration. Results in the form of A-scans and visualization of wave fields were produced for forward scattering by a circular hole in a homogeneous isotropic medium. Transmitter and receiver modals were also incorporated. You and Lord [21] reported improvements from computational point of view, by employing a central-difference formulae for time integration and using a lumped mass matrix. They also studied wave interactions with a rectangular slot and surface breaking cracks in isotropic solids.

A detailed analysis of the various time integration schemes from the point of view of accuracy and speed, was reported by Seron et al [22]. It was concluded that, even though central-difference scheme was the best in terms of computational speed and cost, Newmark's constant average acceleration scheme gives better accuracy.

1.3 Present work and Thesis Layout

In the present work a finite element model to study elastic wave propagation and scattering in thin tubes with cracks has been developed. A methodology has been suggested to for the location and classification of the defects.

Chapter II of the thesis gives the basics of the guided wave propagation in thin layers.

Chapter III describes the finite element modeling of the wave propogation in shells. The problem of spatial and temporal discretization have been discussed.

Chapter IV presents the results for the validation of the computer code and those of the simulations of the tubes with cracks. . The conclusions and the scope for future work are given in chapter V.

Chapter 2

Basics of Guided Wave Propagation In Thin Layers

2.1 Introduction

This chapter deals with a brief discussion of elastic wave propagation in the isotropic thin layers. For plates, exact solution of the equation of motion can be derived from the classical elasticity theory involving infinitesimal deformations. These solutions satisfy the equation of motion and the boundary conditions related to traction-free surfaces. In addition they represent the modes of propagation which exist in simple types of elastic wave guides.

2.2 Propagation in Thin Layers

2.2.1 Integration of equation of elastic motion

The vector differential equation governing the small elastic motions of an isotropic elastic medium in the absence of body forces can be written as

$$\mu \Delta^2 \underline{u} + (\lambda + \mu)\nabla(\lambda.\underline{u}) = \rho\frac{\partial^2 \underline{u}}{\partial t^2} \tag{2.1}$$

where
$\underline{u}$=displacement
t=time
λ,μ=Lame's constants
ρ=density

In the particular problem of analyzing motions in the thin layers, solutions of Eq.(2.1) are to be found consistent with certain boundary conditions(b.c's) to be prescribed. The analysis will lead to a discrete but infinite set of solutions for u which are associated with modes of propagation. The solution of Eq.(2.1) can be recast in a combination of a vector potential function Ψ and a scalar potential Φ such that

$$u = \nabla \Phi + (\nabla \times \underline{\Psi})$$ (2.2)

If Φ and Ψ are solutions to the equations

$$V_D^2 \nabla^2 \Phi = \frac{\partial^2 \Phi}{\partial t^2}$$ (2.3)

$$V_S^2 \nabla^2 \Psi = \frac{\partial^2 \Psi}{\partial t^2}$$ (2.4)

and

$$\nabla . \underline{\Psi} = 0$$ (2.5)

where

$$V_l = (\frac{\lambda + 2\mu}{\rho})^{1/2}$$

and

$$V_s = (\frac{\mu}{\rho})^{1/2}$$ (2.6)

Solutions to the component equations will be sought corresponding to wave motions propagating in the positive axial direction. By assuming a set of solutions of the form

$$\Phi = (A\cos(\alpha x) + B\sin(\alpha x))e^{i(\gamma z - \omega t)}$$

$$\Psi_x = (C\cos(\beta x) + D\sin(\beta x))e^{i(\gamma z - \omega t)}$$

$$\Psi_y = (E\cos(\beta x) + F\sin(\beta x))e^{i(\gamma z - \omega t)}$$

$$\Psi_z = (G\cos(\beta x) + H\sin(\beta x))e^{i(\gamma z - \omega t)} \tag{2.7}$$

Direct substitution of these potential function into Eq.(2.3) and (2.4) indicates that they are the solutions if

$$\alpha^2 + \gamma^2 = \omega^2/V_D^2 \tag{2.8}$$

$$\beta^2 + \gamma^2 = \omega^2/V_S^2 \tag{2.9}$$

Substituting these equations in the displacements obtained from Eq(2.2) and then using the b.c's and the stress strain relationships six equations in A,B,C,D,E,F,G, and H are obtained. The other equations from Eq(2.5).

These eight equations can be considered as a set of homogeneous linear equations in the eight variables A-H. A necessary and sufficient condition for these equations is that the determinant of the coefficients of the variables be zero.

The determinant formed by the these set of equations can be written as a product of four subdeterminants. The equation have solutions for four separate and independent conditions; namely, when any one of the four subdeterminants is equal to zero.
Solution I.
D,G$\neq$0

$$\begin{aligned} u_x &= 0 \\ u_y &= (\beta G + iD)(\sin\beta x)e^{i(z-\omega t)} \\ u_z &= 0. \end{aligned} \tag{2.10}$$

Solution II.

C,H$\neq$0

$$u_x = 0$$
$$u_y = (-\beta H + iC)(\cos \beta x)e^{i(z-\omega t)}$$
$$u_z = 0.$$

$$(2.11)$$

Solution III.

A,F$\neq$0

$$u_x = (-\alpha A \sin \alpha x - iF \sin \beta x)e^{i(z-\omega t)}$$
$$u_y = 0$$
$$u_z = (-\beta F \cos \beta x - iF \cos \alpha x)e^{i(z-\omega t)}.$$

$$(2.12)$$

Solution IV.

B,E$\neq$0

$$u_x = (\alpha B \cos \alpha x - iE \cos \beta x)e^{i(z-\omega t)}$$
$$u_y = 0$$
$$u_z = (-\beta E \sin \beta x + iB \sin \alpha x)e^{i(z-\omega t)}.$$

$$(2.13)$$

For each of the four solutions, the equation formed by setting the appropriate subdeterminant equal to zero is called a frequency equation.

In the discussion of wave motion in plate, it will be convenient to classify the solutions in terms four families of wave motions. In the case of both Solutions I and II, the displacement is transverse to the propogation direction of the wave. Thus, Solution I and II corresponds to shear waves with a particle displacement parallel to the boundary surfaces. Waves of this type are often called SH waves and may be described in terms of antisymmetric SH waves with particle displacements of the form given by Eq(2.9) and symmetric SH waves the form given by Eq(2.10). Fig(2.1) gives the frequency spectrum of symmetric and antisymmetric shear modes in an infinite plate. It is observed from the Fig(2.1) that for all symmetric and anti-symmetric modes the group velocity and phase velocity are functions of frequency, indicating that these velocities become imaginary for values $\omega b/V_s \Phi$. Free propogation in a given mode does not occur at frequencies lower than $\omega b/V_s = r\Phi$. At this point the group velocity in a given mode becomes zero and the frequency at which this happens is called the cut-off frequency of the mode.

The wave motions associated with Solutions III and IV are somewhat more complicated than those associated with the SH modes: first, in the sense that the two displacements components are nonzero, and second, the total wave motion involves a combination of shear and dilatation waves . In Solution III, the particle displacement vectors are symmetrically

arranged with respect to the median plane; so that this is associated with the symmetrical or longitudinal family of modes. The particle displacement vectors in Solution IV are antisymmetrically arranged with respect to the median plane and this solution is associated with the antisymmetrical or flexural family of modes. Fig(2.2) gives the frequency spectrum of longitudinal and flexural modes in an infinite plate.

2.3   Guided waves in tube inspection

There are several popular NDE methods, such as bulk wave ultrasonic, radiography acoustic emission, eddy currents and visual-optics, that have their own advantages and disadvantages for practical inspection work. Recently developed ultrasonic guided wave techniques have some benefits in tubing inspection. The dominant benefit is the penetration ability to inspect an entire length of the tube so that the ultrasonic guided wave technique can locate the defects at any point in tubing without moving the ultrasonic wave transducer. The concept of using guided waves in tubing inspection has been published for many years.

A first concern on the use of ultrasonic guided waves in tubing is to find useful modes. There are at any frequency, at least two guided wave modes available and the number increasess as does the inspection frequency or layer thickness. Theory of elasticity and basic wave mechanics can be used to predict the infinite number of modes that can be generated in a tube. It is known that, two families of Lamb waves exists; the symmetric and the antisymmetric, and the relationship between phase velocity and product of frequency and thickness for different families is given by,

$$\Omega_s(\omega_d, V_{ph}) = \frac{\tan(k_{ts}b/2)}{\tan(k_{tl}b/2)} + \frac{4\beta^2 k_{tl}k_{ts}}{(k_{ts}^2 - \beta^2)^2} = 0 \qquad (2.14)$$

Symmetric Modes

$$\Omega_s(\omega_d, V_{ph}) = \frac{\tan(k_{ts}b/2)}{\tan(k_{tl}b/2)} + \frac{(k_{ts}^2 - \beta^2)^2}{4\beta^2 k_{tl}k_{ts}} = 0 \qquad (2.15)$$

Antisymmetric Modes

where k_{tl} and k_{ts} are given by,

$$k_{tl}^2 = (\tfrac{\omega}{V_l})^2 - \beta^2$$

$$k_{ts}^2 = (\tfrac{\omega}{V_s})^2 - \beta^2$$

The wavenumber, β, is numerically equal to ω/V_{ph} where V_{ph} is the phase velocity of the Lamb wave mode and ω is the circular frequency. The phase velocity of a wave is related to its wavelength by the relation, $V_{ph} = (\omega/2\pi)\lambda$. The quantities V_l and V_s, which represent the longitudinal and shear wave velocities in the bulk material, contains the information on the material properties of the material in which the Lamb waves propagate. The velocities are given by,

$$V_l = (\frac{\lambda + 2\mu}{\rho})^{1/2} \tag{2.16}$$

and

$$V_s = (\frac{\mu}{\rho})^{1/2} \tag{2.17}$$

where λ and μ represent the Lame constants of the layer and ρ represents its mass density.

For a given frequency, Eqn(2.14) and Eqn(2.15) can be considered implicit transcedental functions of phase velocity alone, and they will be satisfied by an infinite number of real, imaginary or complex values of phase velocity. The real solutions for a given frequency represent undamped propogating modes of the structure whereas the imaginary and complex roots represent exponentially decaying modes which do not propogate.

The symmetric Lamb wave modes, governed by Eq.(2.13), have deformation fields which are symmetric about the midplane of the layer, while the anti-symmetric modes, governed by Eq.(2.14) have deformation fields which are anti-symmetric with respect to the midplane of the layer.

For given parameters λ, μ and ρ and a given frequency ω times plate thickness (d) product, the real roots (β) of Eqs. (2.13) and (2.14) represent undamped propagating waves permissible in the layer. There are, at any given ωd a finite number of such roots, with a minimum of two at $\omega d = 0$ and increasing as ω increases. Snell's Law provides the

relationship between the angle of incidence and phase velocity of the guided waves.

$$\Theta_i = \sin^{-1}\left(\frac{V_l}{V_{ph}}\right) \tag{2.18}$$

where V_l represents the velocity of longitudinal waves in the medium containing the incident waves. In practice, where finite sized transducers are used, there is actually a phase velocity spectrum which is excited by the incident wave, not the single phase velocity implied by Eq.(2.17). The range of phase velocities which may be excited by a given transducer depends upon the size of the transducer relative to the wavelength of the generated modes as well as on the pressure distribution across the face of the transducer. Fig(2.3) shows the phase velocity dispersion curve for aluminium. This dispersion curve gives information about the modes that propogate in the plate at the particular frequency, thickness product.The larger the transducer, the more selective it is to the "Snel's law" phase velocity given by Eq.(2.17).

Lamb waves propagate at their group velocities, V_g, as opposed to their phase velocity, V_{ph}, and the two velocities are not, in general, equal. The group velocity dispersion curves for the symmetric or antisymmetric Lamb wave modes can be calculated from the appropriate phase velocity curves by the relation,

$$V_g = \frac{d\omega}{d\beta} = \frac{-\partial\Omega/\partial\beta}{\partial\Omega/\partial\omega} \tag{2.19}$$

where Ω represents Ω_s for the symmetric modes or Ω_a for the antisymmetric modes.

Guided wave field analysis or wave structure through the thickness of tubing is one of the important parameters in selecting modes for a certain purpose. It is by Pilarski et al[25], that points of dominant in plane displacement are achieved for a phase velocity close to the longitudinal wave velocity. Points in the neighbourhood of these special points have dominant in plane components but still some out of plane component which allows coupling and minimal leakage of energy to fluid loaded tubes from the outside if this situation are encountered. From a defect detection point of view, the displacement field analysis give a good explanation of the sensitivity changes to defects. For long range screening purposes, it is better to use modes with less outside sensitivity or/and lower frequencies. Modes with
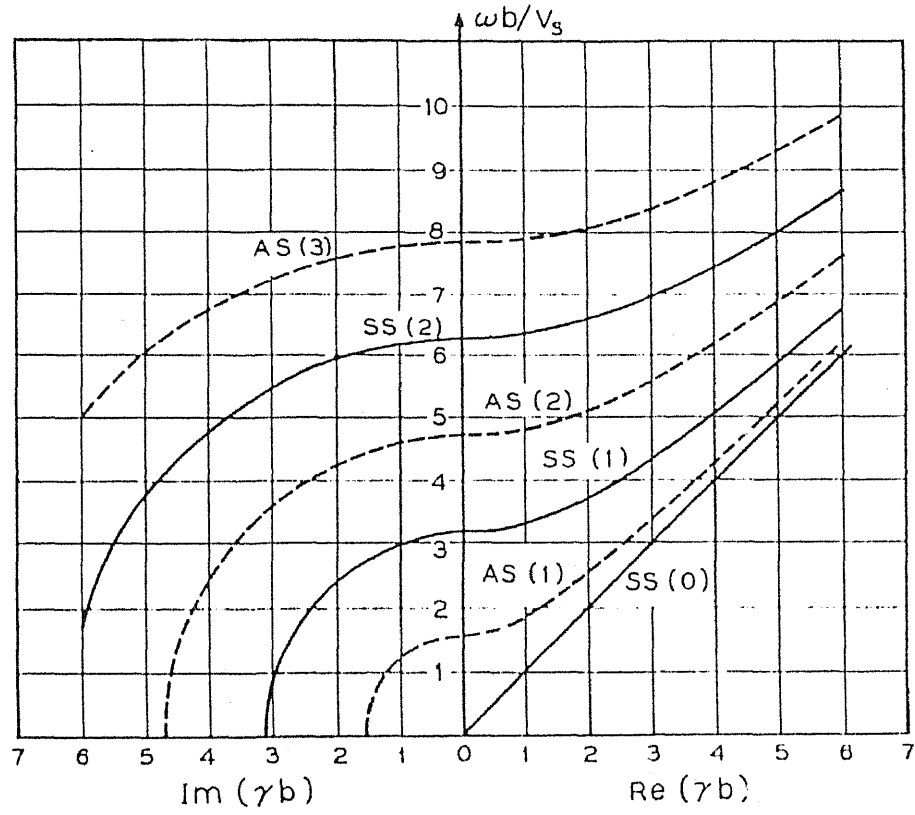
FIG 2.1: FREQUENCY SPECTRUM OF SYMMETRIC AND ANTISYMMETRIC SHEAR MODES IN AN INFINITE PLATE.
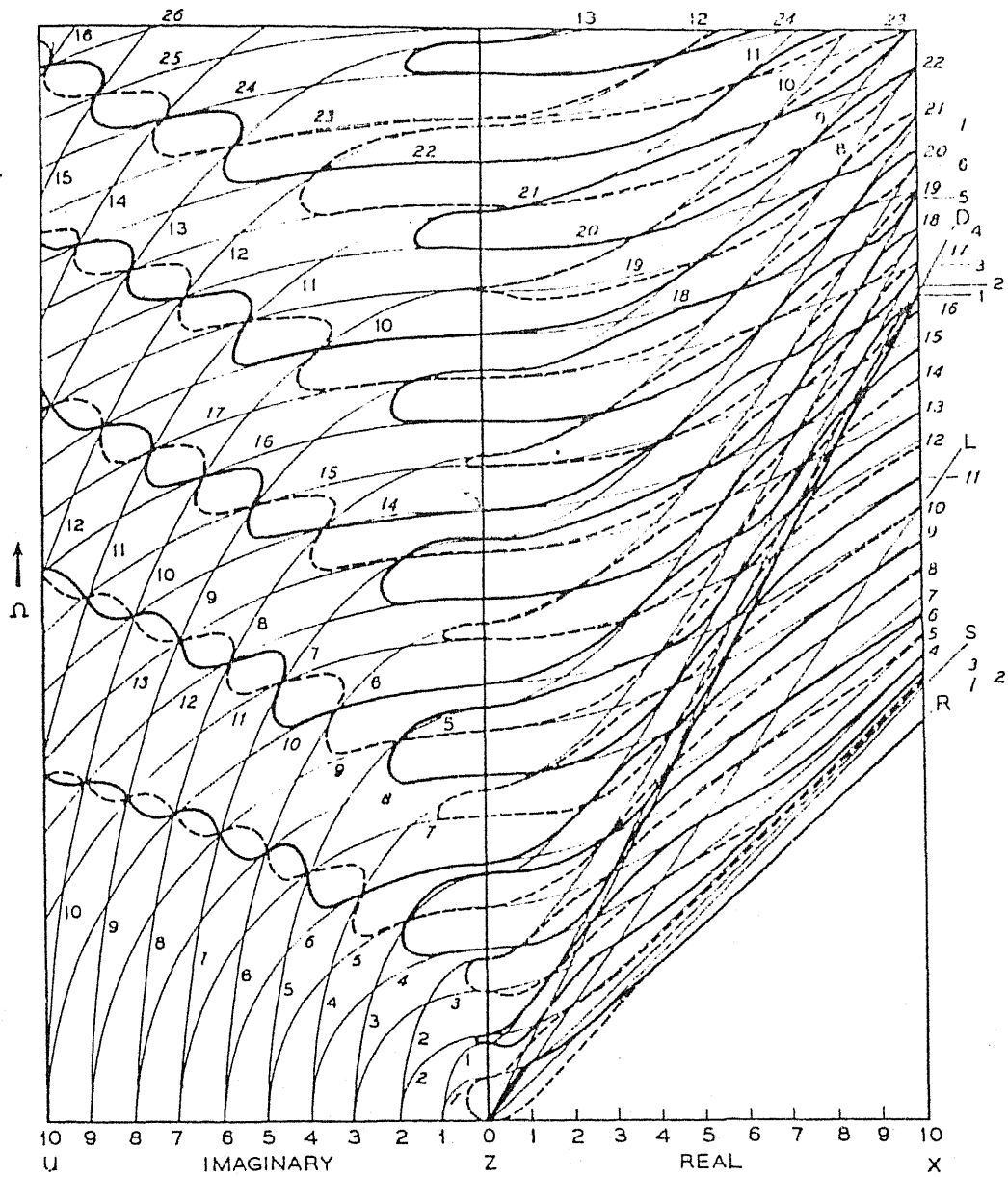
FIG 2.2: FREQUENCY SPECTRUM OF LONGITUDINAL AND FLEXURAL MODES IN AN INFINITE PLATE.

PHASE VELOCITY (mm/μsec) vs **fd (MHz.mm)**

GROUP VELOCITY (mm/μsec) vs **fd (MHz.mm)**
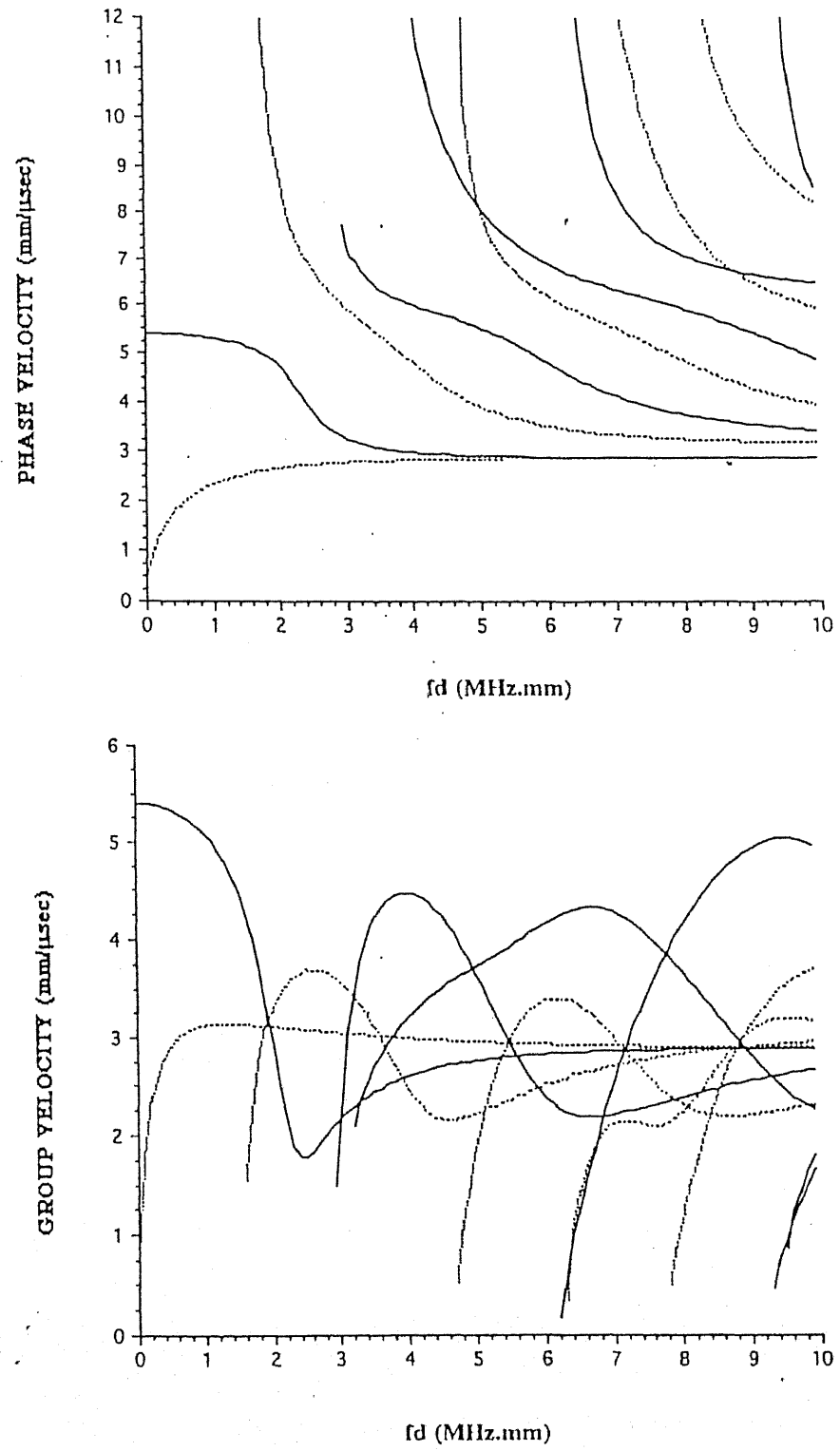
Fig2·3 Phase and group velocity dispersion curves for aluminum single layer.

Chapter 3

Finite Element Modeling of Shells

3.1 Introduction

The development of appropriate methods for the analysis of shell structures is increasingly demanded to ensure the integrity of structural designs. Analytical solutions to shell structures are limited in scope and in general are not applicable to arbitrary shapes, load conditions, irregular stiffening and support conditions, cutouts and many other aspects of practical design. The finite element method has consequently become prominent in the analysis of such shells in view of the ease with which such complexities can be dealt with.

Although finite element procedures have been applied to shell analysis for over years, the search for suitable elements which are readily applicable to general shell structures is still in progress. Three distinct approaches to the finite element representation of shell structures have been employed based on

(i) flat triangular or quadrilateral elements,

(ii) curved elements formulated on the basis of various shell theories and

(iii) elements derived from three-dimensional elements by the use of the degeneration methods.

The first numerical studies of shell problems involved facetting the shell by plane triangular elements, onto which a membrane stiffness was superimposed . The results obtained were found to be satisfactory, but depending on the problem, very fine meshes had to be employed. A number of difficulties and shortcomings arise from the application of flat elements to curved shells, such as the presence of 'discontinuity' in bending moments, which do not appear in the continuously curved actual structures.

In the second approach a classical concept is employed, whereby a shell theory is used as the starting point of the finite element formulation. Different shell theories have been developed from the three dimensional field of equations by incorporating various assumptions assumptions appropriate to the structural behaviour. A variety of finite elements with different degrees of complexity have been formulated for deep and shallow shells. Curved shell elements based on the Kirchhoffs-Love theory guarantee a high solution accuracy but are complicated by convergence and compatibility requirements. In the case of a fully non-linear analysis, additional difficulties arise in the formulation of efficient finite elements due to the unavalibility of a general nonlinear shell theory.

The third approach employed in the formulation of shell elements avoids the complexities of fully general shell theories by discretizing directly the three-dimensional equations of continuum mechanics. Isoparametric elements with independent rotational and displacement degrees of freedom(dof) are employed, in which the three dimensional stress and strain conditions are degenerated to shell behaviour. Although this type of element seemed to be very promising when it was introduced, difficulties later appeared, due to the degeneration process, as the thickness of the element was reduced. A great improvement of the model was achieved by means of the so-called reduced integration technique.

3.1.1   Element Formulation

General

Fig(3.1) shows a solid three-dimensional element based on a quadratic displacement field and and the corresponding quadratic degenerated shell element. Two basic assumptions are adopted in this process: Firstly it is assumed that, even for thick shells, 'normals' to the middle surface remain practically straight after deformation. Secondly, the strain energy corresponding to stresses perpendicular to the middle surface is disregarded, i.e. the stress component normal to the shell mid-surface is constrained to be zero in the constitutive equations.

Five degrees of freedom are specified at each nodal point point, corresponding to its three displacements and the two rotations of the 'normal' at the node. The definition of independent rotational and displacement degrees of freedom permits transverse shear deformation to be taken into account, since rotations are not tied to the slope of the mid-surface.

Coordinate Systems

In the formulation of degenerate shell elements different coordinate systems have to be used. The four coordinate frames employed in the present formulation are as described below.

Global coordinate Set $-x_i$ This is a cartesian coordinate system, freely chosen, in relation to which the geometry of the structure is defined in space. Nodal coordinates and displacements, as well as the global stiffness matrix and applied force vector are referred to this system.

The following notation is used Fig(3.1):

$x_i(i = 1, 3)$ and $x_1 = x, x_2 = y, x_3 = z$

$u_i(i = 1, 3)$ and $u_1 = u, u_2 = v, u_3 = w$

$\bar{x}_i(i = 1, 3)$ is a unit vector in the x_i direction.

Nodal Coordinate set $-\underline{V}_{ik}$

A nodal coordinate system is defined at each nodal point with origin at the reference surface(mid-surface). The vector $\underline{V}_{3k}$ is constructed from the nodal coordinates of the top and bottom surfaces at node k,

$$\underline{V}_{3k} = \underline{x}_k^{top} - \underline{x}_k^{bot} \tag{3.1}$$

where $\underline{x}_k = [\, x_k \ y_k \ z_k \,]^T$

The vector $\underline{V}_{1k}$ is perpendicular to $\underline{V}_{3k}$ and parallel to the global xz-plane,

$$V_{1k}^x = V_{3k}^z, V_{1k}^y = 0.0, V_{1k}^z = -V_{3k}^x \tag{3.2}$$

where the superscripts refer to the vector components in the global coordinate system. The vector $\underline{V}_{2k}$ is perpendicular to the plane defined by $\underline{V}_{1k}$ and $\underline{V}_{3k}$,

$$\underline{V}_{2k} = \underline{V}_{3k} \times \underline{V}_{1k} \qquad (3.3)$$

The unit vectors in the directions of $\underline{V}_{1k}, \underline{V}_{2k}$ and $\underline{V}_{3k}$ are represented by $\bar{\underline{V}}_{1k}, \bar{\underline{V}}_{2k}$ and $\bar{\underline{V}}_{3k}$ respectively .

The vector $\bar{V}_{3k}$ defines the direction of the 'normal' at node k, which is not necessarily perpendicular to the mid-surface at k. Vectors $\bar{\underline{V}}_{1k}$ and $\bar{V}_{2k}$ define the rotations (β_{2k} and β_{1k} respectively) of the corresponding 'normal'. The advantage of this definition for the vector $\underline{V}_{3k}$ (not necessarily perpendicular to the shell mid-surface) is that, as a consequence, there are no gaps or overlaps along element boundaries.

Curvilinear Coordinate Set - ξ,η,ζ

In this system ξ and η are two curvilinear coordinates in the middle plane of the shell element and ζ is a linear coordinate in the thickness direction. It is assumed that ξ, η and ζ vary between -1 and +1 on the respective faces of the element. The relations between the curvilinear coordinates (ξ, η, ζ) and the global coordinates (x,y,z) are given by expressions (-), which later define the element geometry. It should be noted that the ζ-direction is only approximately perpendicular to the shell middle surface, since ζ is defined as a function of $\bar{V}_{3k}$.

Local coordinate Set -x_i'

This is a Cartesian coordinate system defined at the sampling points where in ? stresses and strains are to be calculated. Various directions are obtained by using the relations given below,

$$x_3' = \begin{bmatrix} \frac{\partial x}{\partial \xi} \\ \frac{\partial y}{\partial \xi} \\ \frac{\partial z}{\partial \xi} \end{bmatrix} \times \begin{bmatrix} \frac{\partial x}{\partial \eta} \\ \frac{\partial y}{\partial \eta} \\ \frac{\partial z}{\partial \eta} \end{bmatrix} \qquad (3.4)$$

$$\underline{x}'_1 = \begin{bmatrix} \frac{\partial x}{\partial \xi} \\ \frac{\partial y}{\partial \eta} \\ \frac{\partial z}{\partial \zeta} \end{bmatrix} \tag{3.5}$$

$$\underline{x}'_2 = \underline{x}'_3 \times \dot{\underline{x}}'_1 \tag{3.6}$$

The local coordinate system varies along the thickness for any 'normal' with this variation depending on the the shell curvature and variable thickness.

Element Geometry

The global coordinates of pairs of points on the top and bottom surface at each node are usually input to define the element geometry. In the isoparametric formulation the coordinates of a point within the element are obtained by applying the element shape functions to the nodal coordinates,

$$x_i = \sum_{k=1}^{n} N_k \frac{(1+\eta)}{2} x_{ik}^{top} + \sum_{k=1}^{n} N_k \frac{(1-\eta)}{2} x_{ik}^{bot} \tag{3.7}$$

where i=1,3 refers to the three global directions,

n - is the number of nodes per element,

$N_k(\xi, \eta)(k = 1, n)$ are the element shape functions corresponding to the surface ζ=constant,

h_k - is the shell thickness at node k, i.e. the respective 'normal' length,

ξ, η, ζ - are the curvilinear coordinates of the point under consideration.

Displacement Field

The element displacement field can be expressed as,

$$u_i = \sum_{k=1}^{n} u_{ik}^{mid} + \sum_{k=1}^{n} N_k \zeta \frac{h}{2} \begin{bmatrix} \bar{V}_{1k} & \bar{V}_{2k} \end{bmatrix} \begin{bmatrix} \beta_{1k} \\ \beta_{2k} \end{bmatrix} \tag{3.8}$$

The contribution to the global displacements from a given node k is:

$$\begin{bmatrix} u \\ v \\ w \end{bmatrix} = \begin{bmatrix} N_k & 0 & 0 & N_k \zeta \frac{h}{2} V_{1k}^x & -N_k \zeta \frac{h}{2} V_{2k}^x \\ 0 & N_k & 0 & N_k \zeta \frac{h}{2} V_{1k}^y & -N_k \zeta \frac{h}{2} V_{2k}^y \\ 0 & 0 & N_k & N_k \zeta \frac{h}{2} V_{1k}^z & -N_k \zeta \frac{h}{2} V_{2k}^z \end{bmatrix} \begin{bmatrix} u_k \\ v_k \\ w_k \\ \beta_{1k} \\ \beta_{2k} \end{bmatrix} \tag{3.9}$$

Calculation of Strains

In order to easily deal with the shell assumption of zero normal stress in the z' - direction $\sigma_{z'} = 0$, the strain components should be defined in terms of the local system of axes x_i'. The five significant strain components are,

$$\underline{\epsilon} = \begin{bmatrix} \epsilon_{x'} \\ \epsilon_{y'} \\ \gamma_{x'y'} \\ \gamma_{x'z'} \\ \gamma_{y'z'} \end{bmatrix} = \begin{bmatrix} \frac{\partial u'}{\partial x'} \\ \frac{\partial v'}{\partial y'} \\ \frac{\partial u'}{\partial y'} + \frac{\partial v'}{\partial x'} \\ \frac{\partial u'}{\partial z'} + \frac{\partial w'}{\partial x'} \\ \frac{\partial v'}{\partial z'} + \frac{\partial w'}{\partial y'} \end{bmatrix} \tag{3.10}$$

where u', v' and w' are the displacement components in the local system x_i'.

Calculation of Stresses

Taking into consideration the assumption of zero stress in the direction perpendicular to the shell mid-surface ($\sigma_{z'} = 0$), the five stress components in the local system are:

$$\underline{\sigma} = \begin{bmatrix} \sigma_{x'} \\ \sigma_{y'} \\ \tau_{x'y'} \\ \tau_{x'z'} \\ \tau_{y'z'} \end{bmatrix} \qquad (3.11)$$

Layered model

If the shell is built up from a series of different materials, such that the material properties(and stress) are discontinuous functions of ζ, an appropriate integration through the thickness has to be carried out. Here layered approach is employed, wherein a midpoint rule integration scheme is adopted for each layer. Each layer contains stress points on its mid-surface. The stress components of the layer are computed at these stress points and are assumed to be constant over the thickness of each layer, so that the actual stress distribution of the shell is modeled by a piecewise constant approximation. The specification of layer thickness in terms of curvilinear coordinate, ζ, permits the variation of the layer thickness as the shell thickness varies.

The stress resultants are obtained by integrating the corresponding stress components with respect to the thickness coordinate:

-normal forces,

$$N_x = \int_{-h/2}^{h/2} \sigma_x dz = h/2 \sum_{i=1}^{n} \sigma_x^i \Delta \zeta^i$$

$$N_y = \int_{-h/2}^{h/2} \sigma_y dz = h/2 \sum_{i=1}^{n} \sigma_y^i \Delta \zeta^i \qquad (3.12)$$

-bending moments

$$M_x = \int_{-h/2}^{h/2} \sigma_x z dz = -h^2/4 \sum_{i=1}^{n} \sigma_x^i \zeta^i \Delta \zeta^i$$

$$M_y = \int_{-h/2}^{h/2} \sigma_y z \, dz = -h^2/4 \sum_{i=1}^{n} \sigma_y^i \zeta^i \Delta \zeta^i \qquad (3.13)$$

$$M_{xy} = \int_{-h/2}^{h/2} \sigma_{xy} z \, dz = -h^2/4 \sum_{i=1}^{n} \sigma_{xy} i \zeta^i \Delta \zeta^i$$

-shear forces

$$Q_x = \int_{-h/2}^{h/2} \tau_{xz} \, dz = h/2 \sum_{i=i}^{n} \tau_{xz}^i \Delta \zeta^i$$

$$Q_y = \int_{-h/2}^{h/2} \tau_{yz} \, dz = h/2 \sum_{i=1}^{n} \tau_{yz}^i \Delta \zeta^i \qquad (3.14)$$

where n (i=1,n) is the number of layers.

In the present code the strain matrix $\underline{B}$ is calculated at the mid-surface of each layer: the element stiffness matrix $\underline{K}^e$ and the internal force $\underline{f}^e$ are thus defined as follows:

$$\underline{K}^e = \int \int_{-1}^{+1} \underline{B}^T \underline{D} \underline{B} \, d\zeta \, dA \qquad (3.15)$$

$$\underline{f}^e = \int \int_{-1}^{+1} \underline{B}^T \underline{\sigma} J \, d\zeta \, dA \qquad (3.16)$$

where

$$\int \dots dA = \int \int_{-1}^{+1} \dots d\eta \xi \quad \text{(integration on layer midsurface)}$$

and J is the determinant of the Jacobin matrix. This process of integration in the thickness direction is computationally more expensive, but is more appropriate for thick and

variable thickness problems in which the variation of the local system of axes, as well as the variation of the Jacobian matrix through the shell thickness must be taken into account.

Element Mass Matrix

Due to computational convenience and simplicity lumping of mass matrices is considered. Te essential requirement of mass preservation is given as:

$$\sum_i \tilde{M}_{ii} = \int_\Omega \rho \, d\Omega \qquad (3.17)$$

where $\tilde{M}_{ii}$ is the diagonal of the lumped mass matrix $\tilde{M}$.
The approximation used here for mass lumping is Diagonal scaling procedure. This method satisfies the essential requirement given by the above equation.
In this method

$$\tilde{M}_{ii} = a M_{ii}$$

with a so adjusted that Eq(3.-) is satisfied. By following this method for our present analysis the mass at the end nodes and and at the central nodes will be 1/36 and 8/36 times that of the total mass respectively.

3.2   Time Discretization

The system of linear, second order, ordinary differential equations with constant coefficients has to be integrated in the time interval (0,T) by discretizing the time variables as $t_n \doteq n' \Delta t$, $0 \leq n' \leq N$ where $\Delta t = T/N$.

3.2.1   Central Difference Scheme

In the central difference scheme it is assumed that

$$\frac{^t \partial U}{\partial t} = \frac{1}{2\,\Delta t}(^{t+\Delta t}U - {}^{t-\Delta t}U)$$

$$\frac{^t\partial^2 U}{\partial t^2} = \frac{1}{\Delta t^2}\{^{t-\Delta t}U - 2\,^tU + \,^{t+\Delta t}U\} \tag{3.18}$$

Consider the equation of motion at time t, i.e.,

$$M[\frac{^t\partial^2 U}{\partial t^2}] + K\,^tU = \,^tF \tag{3.19}$$

Substitution of Eq.(3.10) into (3.11) gives

$$(\frac{1}{\Delta t^2}M)\,^{t+\Delta t}U = \,^tF - (K - \frac{2}{\Delta t^2}M)\,^tU - (\frac{1}{\Delta t^2}M)\,^{t-\Delta t}U \tag{3.20}$$

from which one solve for $^{t+\Delta t}U$, given the initial conditions.

It should be noted that the solution of $^{t+\Delta t}U$ is based on the equilibrium conditions at time t. For this reason this integration procedure is called an explicit integration method. It is noted that such an integration scheme do not require a factorization of the stiffness matrix in the step-by-step solution. So if the mass matrix is diagonalized the assembly of the mass and stiffness matrix are not required. This is the important advantage of central difference scheme from computational point of view, even though it is inferior to the implicit Newmark's scheme which uses the equilibrium conditions at time $t + \Delta t$.

With a diagonal mass matrix above equation can be simplified as

$$^{t+\Delta t}U_i = \,^t\hat{R}_i(\frac{\Delta t^2}{m_{ii}}) \tag{3.21}$$

where

$$^t\hat{R} = \,^tF - (K - \frac{2}{\Delta t^2}M)\,^tU - (\frac{1}{\Delta t^2}M)\,^{t-\Delta t}U \tag{3.22}$$

3.2.2 Newmark's Method

The Newmark's algorithm under the assumption of constant-average acceleration is as follows,

$$\frac{^{t+\Delta t}\partial U}{\partial t} = \frac{^{t}\partial U}{\partial t} + [(1-\delta)\frac{^{t}\partial^2 U}{\partial t^2} + \delta\frac{^{t+\Delta t}\partial^2 U}{\partial t^2}]\Delta t$$

$$^{t+\Delta t}U = {}^{t}U + \frac{^{t}\partial U}{\partial t}\Delta t + [(1/2-\alpha)\frac{^{t}\partial^2 U}{\partial t^2} + \alpha\frac{^{t+\Delta t}\partial^2 U}{\partial t^2}]\Delta t^2 \qquad (3.23)$$

where α and δ are parameters that can be determined to obtain an unconditionally stable scheme known as the constant average acceleration method, in which $\delta = 1/2$ and $\alpha = 1$.

In addition to the above difference equations, for solution of displacements, velocities and acceleration, the equilibrium equations at time $t + \Delta t$ are considered:

$$M\frac{^{t+\Delta t}\partial^2 U}{\partial t^2} + K\,{}^{t+\Delta t}U = {}^{t+\Delta t}F \qquad (3.24)$$

Using the above two equations we obtain the following equations for $^{t+\Delta t}U$,

$$[M + \frac{\Delta t^2}{4}K]\,{}^{t+\Delta t}U = \frac{\Delta t^2}{4}\,{}^{t+\Delta t}F + M[{}^{t}U + \Delta t\frac{^{t}\partial U}{\partial t} + \frac{\Delta t^2}{4}\frac{^{t}\partial^2 U}{\partial t^2}] \qquad (3.25)$$

It is seen that this is an implicit scheme and requires the factorization of the stiffness matrix. This is reported to be more accurate than the central difference scheme.

a)

Global Coord. System

Nodal Coord. System
at Node k

b)

Surface ζ = constant

Surface η = constant

Local Coord. System
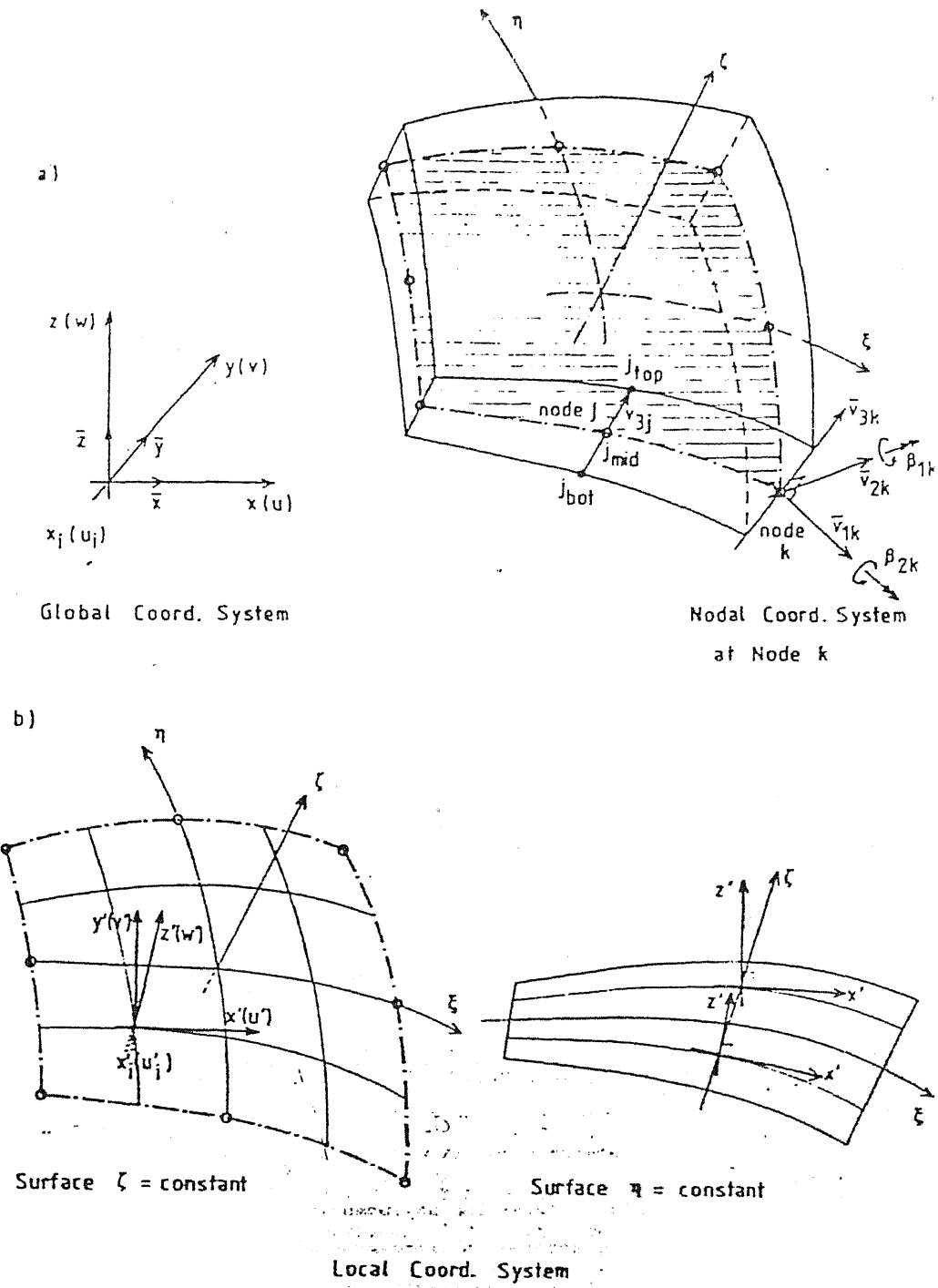
FIG 3.1: ELEMENT GEOMETRY AND COORDINATE SYSTEMS.

Chapter 4

Results and Discussion

This chapter discusses the results of guided wave propagation in a few problems using FEM as discussed in earlier chapters. The emphasis is on its application as a Non-Destrective technique(NDT) to detect cracks.

4.1 Validation of the code

In order to verify the code an example of cylindrical barrel vault was considered. The geometry and physical details are given in Fig(4.1). The barrel is supported on rigid diaphragms and is loaded by its own weight. In the present analysis 16(4 × 4) degenerated shell elements are used. Fig(4.2) shows some comparitive results, obtained by using the present code with that of exact results. The results are almost identical with the exact ones.

Fig(4.2a) gives the vertical deflection of the central section of the vault, Fig(4.2b) gives horizontal displacement of the support.

4.2 Wave Propogation in Tubes

4.2.1 Details of Specimen geometry and loading

The domain modelled is a thin tube of outer diameter 18.9mm, 1.22mm thick and 350mm long. The specimen geometry is shown in Fig(4.3). Two different coordinate frames are used in the analysis viz., cartesian coordinate system and polar coordinatesystem. Fig(4.3) also contains the the two coordinate frames viz., cylindrical(r,θ,y) and cartesian(X,Y,Z) coordinate frames with respect to the specimen.

For convenience,the output of the Finite element code are expressed in radial, circumferential and axial components as shown in Fig(4.3).

As seen in the Fig(4.3) ultrasonic pulse is applied at three locations viz., S_1,S_2 and S_3 which are circumferentially 120 degrees apart. The loads F_1,F_2 and F_3 are applied in the tangential plane at the loading points. Load at each of the three source locations is at an angle of 20 degrees to the axial plane. The loading as shown in the Fig(4.3) is specified in cartesian coordinate system. The transducer is modelled with a cosine pulse of one full cycle. Fig(4.4) contains the input at the three source locations in the cartesian coordinates.

Eight-noded degenerated shell elements have been used. For time integration central difference and Newmark's time integration scheme is used.

The properties of the material are taken as follows:

E=69.0 Gpa, G=26.4 Gpa, =0.33, $\rho = 1800 kg/m^3$

The compressional, shear wave velocities in the material can be found as

$C_l = 7.20 km/sec$, $C_s = 3.80 km/sec$, $C_R = 3.10 km/sec$

The transducer pulse is modelled as

$$f(t) = (1 - cos(2\Pi f)) \quad 0 \leq t \leq 12.5 \ \mu sec$$

$$= 0 \qquad\qquad t > 12.5 \ \mu sec$$

A frequency of 0.1 MHz is selected, because for this product of frequency and thickness only two modes of guided waves exists as seen from the dispersion curves for aluminium in Fig(2.3). For this frequency the corresponding wave lengths are

$\lambda_l = 67.5 mm$, $\lambda_s = 31.0 mm$, $\lambda_R = 29.0 mm$

Table(4.1) gives details of the five simulations performed.

First simulations are performed on a defect free specimen, later two specimens with circumferential cracks and two specimens with longitudinal crack at various axial and angular

First simulations are performed on a defect free specimen, later two specimens with circumferential cracks and two specimens with longitudinal crack at various axial and angular positions are considered.

Table(4.1)

Cases	No.of elem	No.of nodes	Axial location of crack(mm)	Angular location of crack(mm)
1.Defect free	720	2208	-	-
2.Circumferential crack	720	2211	175	165-195
3.Circumferential crack	720	2211	233	210-240
4.Circumferential crack	720	2211	163.3-186.6	180
5.longitudinal crack	720	2211	128.3-151.6	120

In all the simulations performed the load is applied at three locations which are circumferentially 120 degrees apart. The load at all the source locations was in the tangential plane.

The finite element output includes radial(u), circumferential(v), axial displacements(w) at the three source locations, at every time step.

4.3 Propogation in defect-free specimen

This simulation is performed to determine the movement of the wave propogation in the specimen and to verify the the speed of the wave in the axial and in the circumferential direction. Fig(4.3) gives the details of the geometry of the specimen and loading.

Fig(4.5) and Fig(4.6) show the circumferential and axial dispalcement field in the domain at different times after the application of the pulse. The displacement fields are plotted as isometric views to bring out the features. As the loading is in the tangential plane, displacement field is very small in the radial direction and hence those plots are not shown. The evolution and propogation of the deformations are clearly seen. In particular from Fig(4.5) and Fig(4.6) it can be seen that the axial displacements with the selected set

of loading directions, the pulse is able to effectively scan the entire surface of the specimen. As seen from the plots the finite element predictions match well with the theoretical arrival times. As the load and the geometry is symmetric the A-scan plot at the three source locations is the same as seen from Fig(4.7) and Fig(4.8). As seen from the snapshots the wave speed in the axial direction is found to be 3755.55 m/sec, which is equal to the shear speed of the wave. The wave speed in the circumferential direction is found to be 2545.45 m/sec. Fig(4.7) and Fig(4.8) contains the A-scan plots at the three source locations.

It is seen from the A-scan plots in the circumferential direction that the wave doesn't attenuate after the completion of the application of the load because it is the surface wave which is propogating in the circumferential direction, this is in contrast to the pulse in the axial direction which attenuates soon after the completion of the application of the load. The reflected pulse from the other end of the tube is clearly seen in Fig(4.7). In Fig(4.8) the reflected pulse cannot be observed clearly as the magnitude of the reflected surface wave is too small in comparision to the input pulse.

4.4   Wave interaction with a Circumferential crack

The objective here is to simulate wave propogation in tubes with circumferential cracks and suggest a method to determine the axial and angular location of the crack. The simulations are performed on two specimens with different angular and axial locations. Fig(4.9) and Fig(4.16) give the geometry of the specimen, loading as well as the location of the crack. In order to analyse the plot of and hence to find the location of the crack, A-scan plot of differences of displacements at the three locations has been attempted. This becomes necessary as the magnitude of the reflected pulse is much smaller than the magnitude of the original pulse. it is observed that the magnitude of the reflected pulse is in the order of 10^{-8}, when compared to the original pulse which is of the order of 10^{-5}. These plots give clear information about the location of the crack. As load is symmetric the A-scan plot of from all the source locations should be exactly the same unless there is some flaw which creates unsymmetry in the geometry. From the known speed of the propogation of the wave and the time taken for the reflection from the crack(flaw), axial location is determined for various cases separately. It should be noted that the time obtained from the difference plots is the time taken by the wave to travel from the source to the flaw and back to the source. From the difference of the A-scan plot one can find angular location of the crack too.

4.4.1 Case(i): Crack located at 175 mm length and 180° angle

Fig(4.9) gives the geometry of the specimen, location and orientation of the crack and the loading. The snapshots of the simulation are shown in Fig(4.10) and Fig(4.11). Fig(4.12) shows the A-scan plots of displacement difference at all the three source.locations. Fig(4.10) and Fig(4.11) shows the propogation of the wave. Fig(4.12) and Fig(4.13) give the A-scan plots at all the source locations. Fig(4.14) which give the A-scan plot of differences of$(v_i - v_j)$ at various source locations. From these plots it can be seen that the displacement suddenly becomes significant at time 137 μ sec. This corresponds to the time at which the reflected wave from the crack surface reaches the source. From the obtained time of travel, the axial location of the crack can be obtained. Table(4.2) below gives the details of the simulation as given by the axial difference plots . If the A-scan plots$(v_i - v_j)$ difference are closely examined, first plot which shows difference $(v_1 - v_2)$ and the second plot which shows the difference $(v_2 - v_3)$ are similar, i.e, they are in phase and almost of same magnitude. This depicts that angular location of the crack is some where in between those of source 1 and 3 along the direction of wave travel(i.e along the direction of loading) and preferrably equidistant from both of them, same is the case with plots three and one.

Table(4.2)

Time of travel of reflected pulse(μ sec)	Axial Location (estimated)	Anngular Location (estimated)	Axial Location (calculated)	Angular Location (calculated)
137	175	165-195	174.36	170-190

4.4.2 Case(ii): Crack located at 233.3 mm length and 225° angle

Fig(4.16) gives the geometry of the specimen, location and orientation of the crack and the loading. The snapshots of the simulation are shown in Fig(4.17) and Fig(4.18). Fig(4.21) shows the A-scan displacement difference plots at all the three source locations. Fig(4.17) and Fig(4.18) shows the propogation of the wave. Fig(4.19) and Fig(4.20) give the A-scan plot of displacements at the three source locations. Fig(4.21) gives the difference of A-scan plot of$(v_i - v_j)$ difference at the source locations in the circumferential direction from which it can be clearly seen that the displacements becomes significant at time 175 μ sec. This is the time at which the reflected wave from the crack surface reaches the source. From the obtained time of travel, the axial location of the crack can be obtained. Table(4.3) below gives the details of the simulation as given by the axial difference plots. to

find some information about the angular location A-scan plot of displacement differences are to be observed closely. Plots three and one are in the same direction with a small phase difference. They have much variation in there peak values, plot three having higher peak value than that of plot one. This shows that the angular location of crack is between source location 3 and 1 and closer to source location 3.

Table(4.3)

Time of travel of reflected pulse(μ sec)	Axial Location (estimated)	Anngular Location (estimated)	Axial Location (calculated)	Angular Location (calculated)
175	233.33	210-240	222.72	230-270

4.5 Wave interaction with an Axial crack

The objective here is to simulate wave propogation in tubes with axial cracks and determine the axial and angular location of the crack. In case of axial crack the reflections are sharp as compered to the Circum ferential cracks. The simulations are performed on two specimens with varying axial and angular locations.

4.5.1 Case(i): Crack located at 175 mm length and 180° angle

Fig(4.23) gives the geometry of the specimen, location and orientation of the crack and the loading. The results of the simulation are shown in Fig(4.24) and Fig(4.25). Fig(4.26) shows the A-scan displacement difference plots at all the three source locations. Fig(4.24) and Fig(4.25) shows the propogation of the wave. Fig(4.26) and Fig(4.27) give the A-scan plot of the difference at the three source locations. Fig(4.27) give the difference of A-scan plot of at the source locations of $(v_i - v_j)$ from which it can be clearly seen that the displacements becomes significant at time 135 μ sec. This is the time at which the reflected wave from the crack surface reaches the source. From the obtained time of travel, the axial location of the crack can be obtained. Table(4.4) below gives the details of the simulation as given by the axial difference plots. In order to find some information about the angular location A-scan plot of displacement differences need to be observed closely. In Fig(4.27) plots two and three are in the same direction with a small phase difference. This depicts that the crack is between source 2 and 1 and close to source location 2. It is also observed that the plot one is exactly 180 degrees apart from that of two and three, this means that

the crack is very close to source two.

Table(4.4)

Time of travel of reflected pulse(μ sec)	Axial Location (estimated)	Anngular Location (estimated)	Axial Location (calculated)	Angular Location (calculated)
135	175	180	171.81	170-190

4.5.2 Case(ii): Crack located at 140 mm length and 120° angle

Fig(4.30) gives the geometry of the specimen, location and orientation of the crack and the loading. The snapshots of the simulation are shown in Figs(4.31) and (4.32). Fig(4.35) shows the A-scan displacement difference plots at all the three source locations. Fig(4.33) and Fig(4.34) shows the propogation of the wave. Fig(4.33) and Fig(4.34) give the A-scan plot of at the three source locations. Fig(4.35) gives the difference of A-scan plot of $(v_i - v_j)$source locations in the circumferential direction from which it can be clearly seen that the displacements suddenly became significant at time 135 μ sec. This is the time at which the reflected wave from the crack surface reaches the source. From the obtained time of travel, the axial location of the crack can be obtained. Table(4.5) below gives the details of the simulation as given by the circumferential difference plots. In order to find some information about the angular location A-scan plot of displacement difference are to be observed closely. Plots three and one are in the same direction with a small phase difference. This may depict that the crack is between source 3 and 2 and close to 2.

Table(4.5)

Time of travel of reflected pulse(μ sec)	Axial Location (estimated)	Anngular Location (estimated)	Axial Location (calculated)	Angular Location (calculated)
100	140	120	128	100-140

Z,W   Y,V

X,U

supported by
rigid diaphragm
u=0
w=0

Free edge

7.6 m

R=7.6 m

40

supported by
rigid diaphragm
u=0
w=0
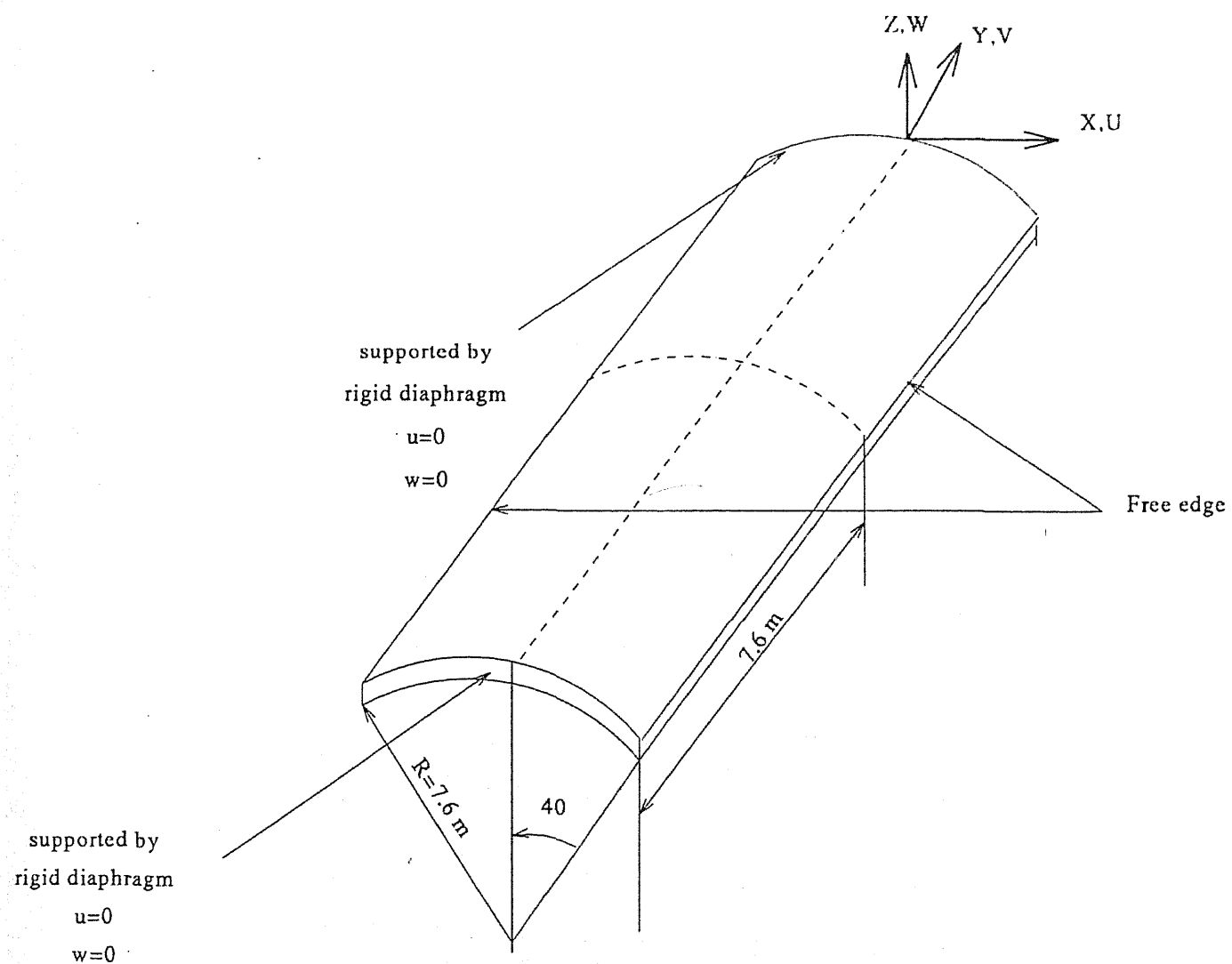
FIG 4.1: CYLINDRICAL BARREL VAULT
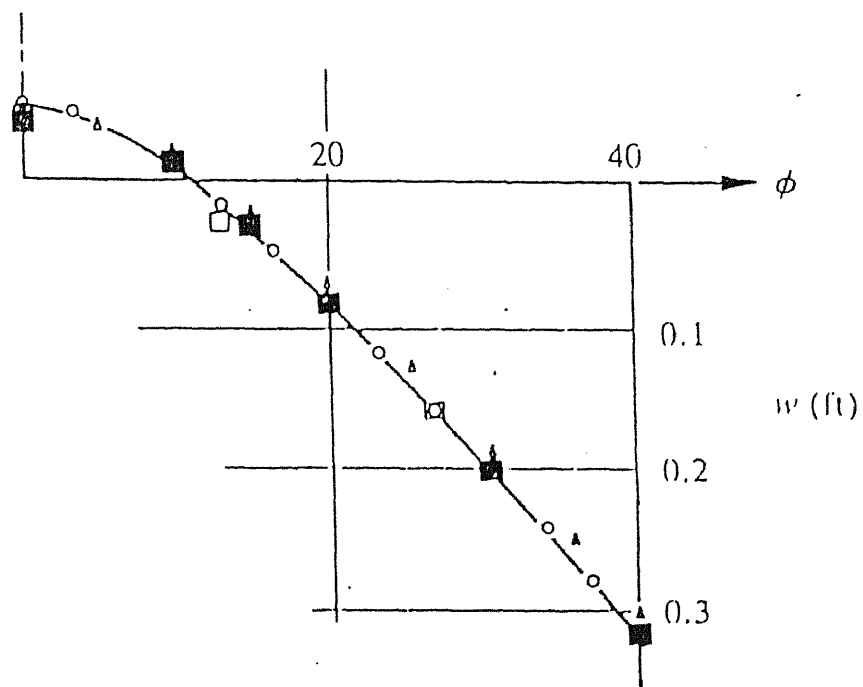
Fig 4·2a Vertical displacement of central sections
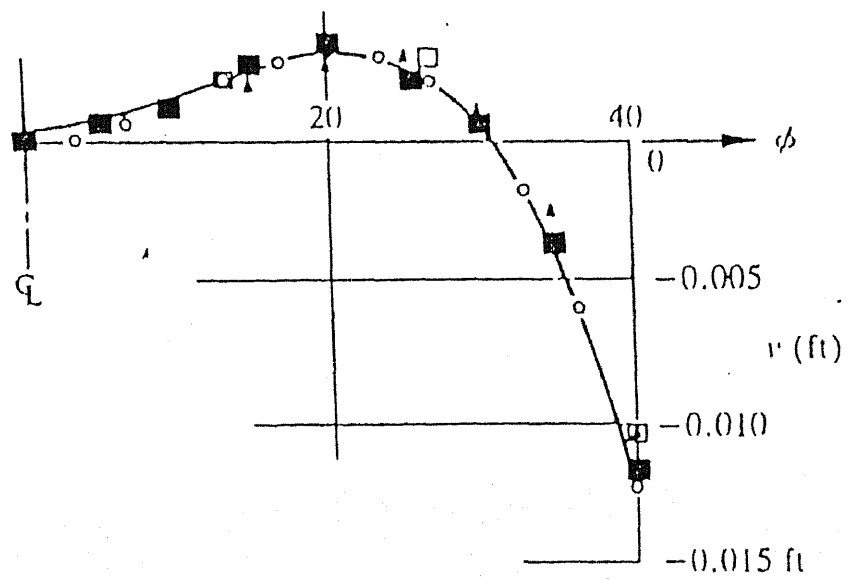
Fig 4·2b Longitudinal displacement of support
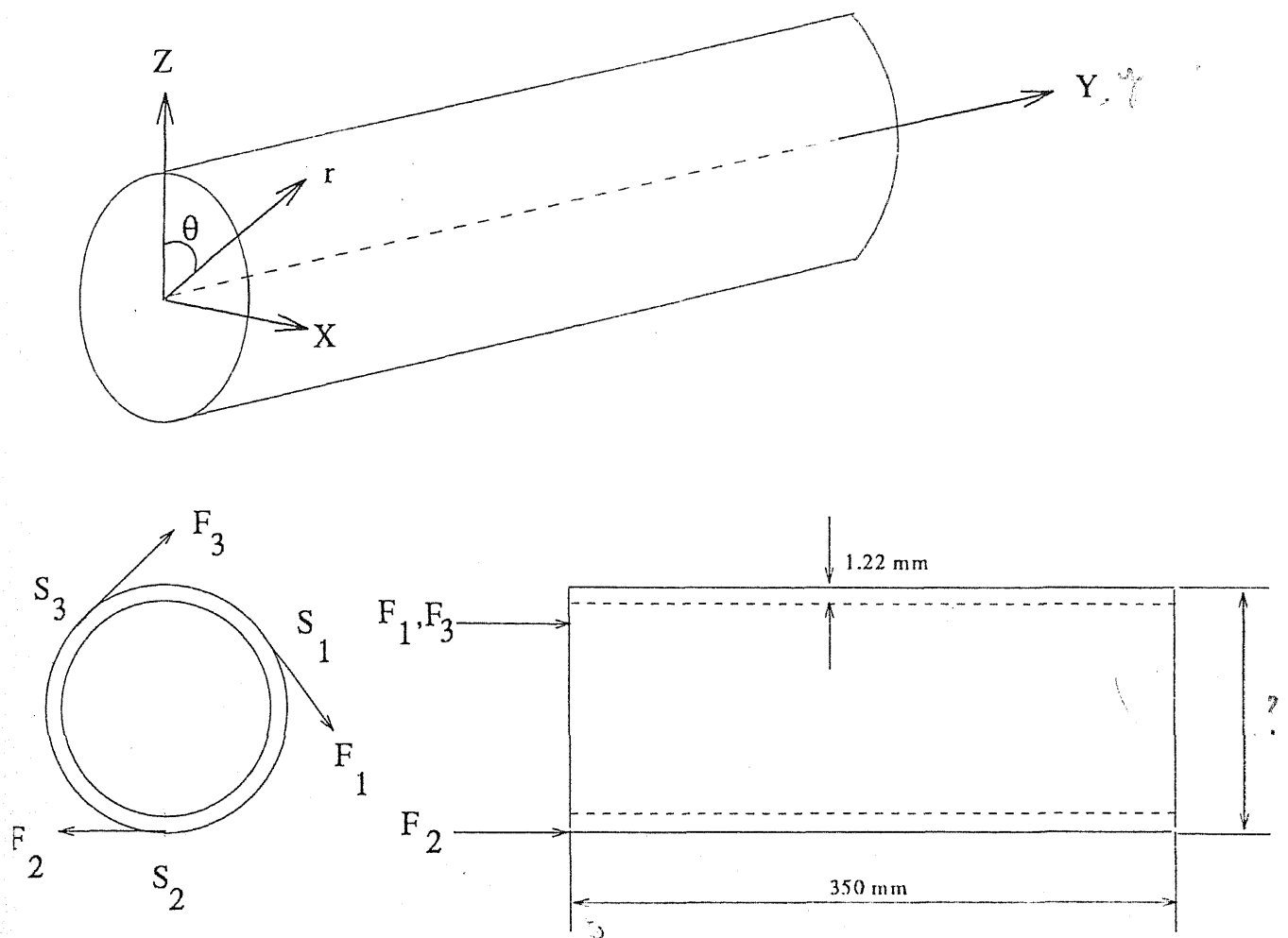
FIG 4.3: SPECIMEN GEOMETRY AND CO-ORDINATE SYSYTEM
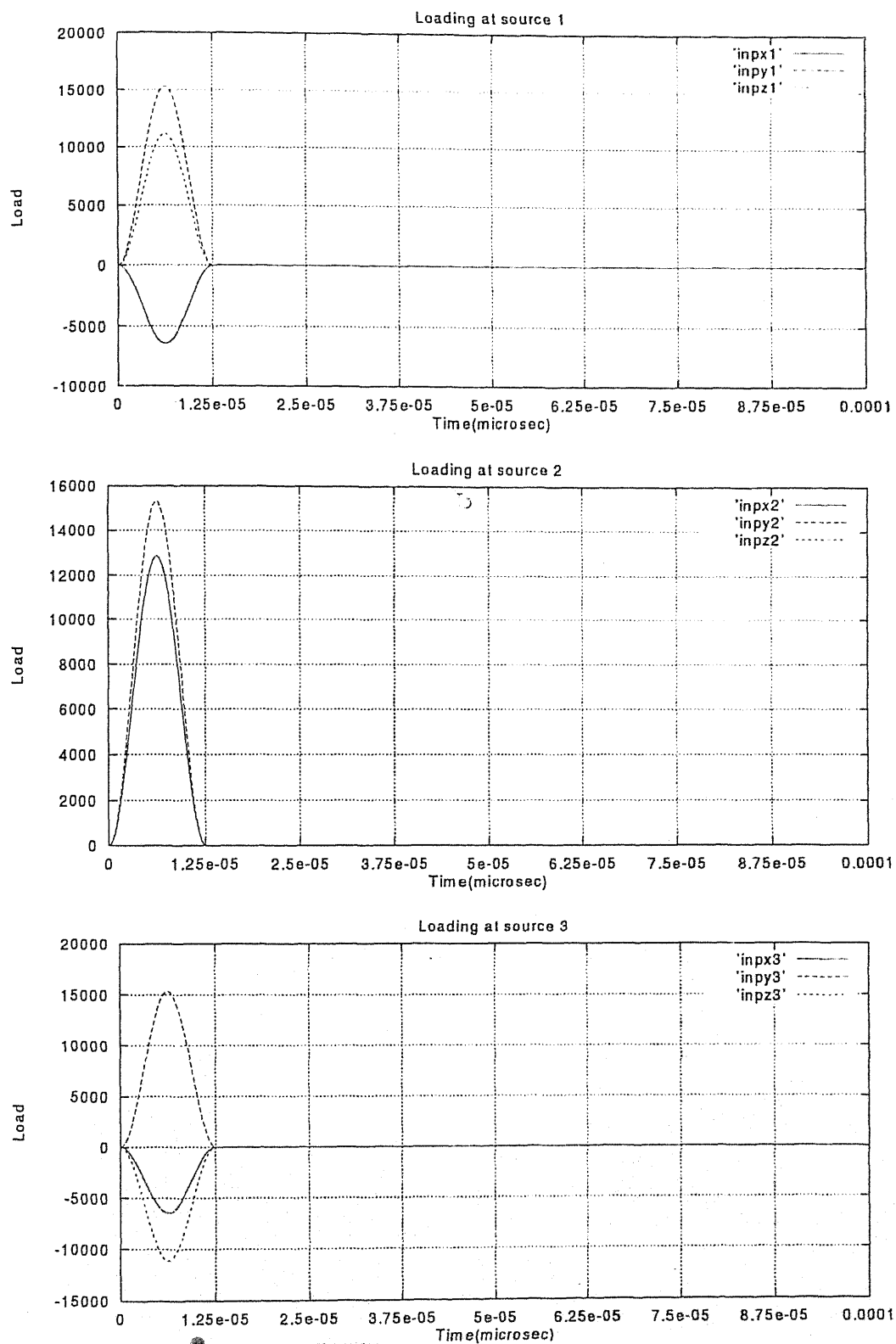
FIG 4.4: INPUT PULSE AT THE THREE SOURCE LOCATIONS
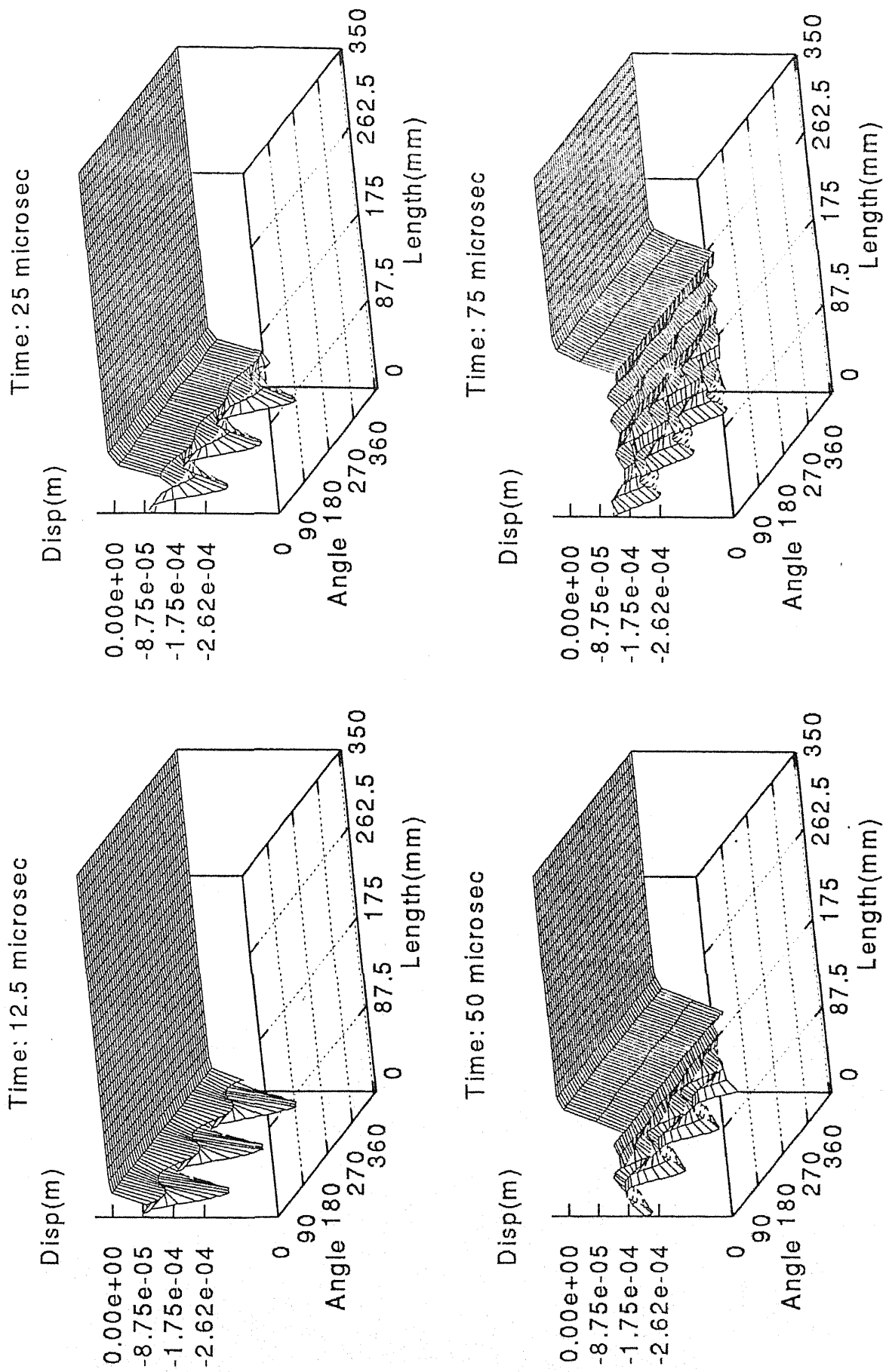
FIG 4.5: SNAPSHOTS OF CIRCUMFERENTIAL DISPLACEMENTS

DEFECT FREE SPECIMEN

43
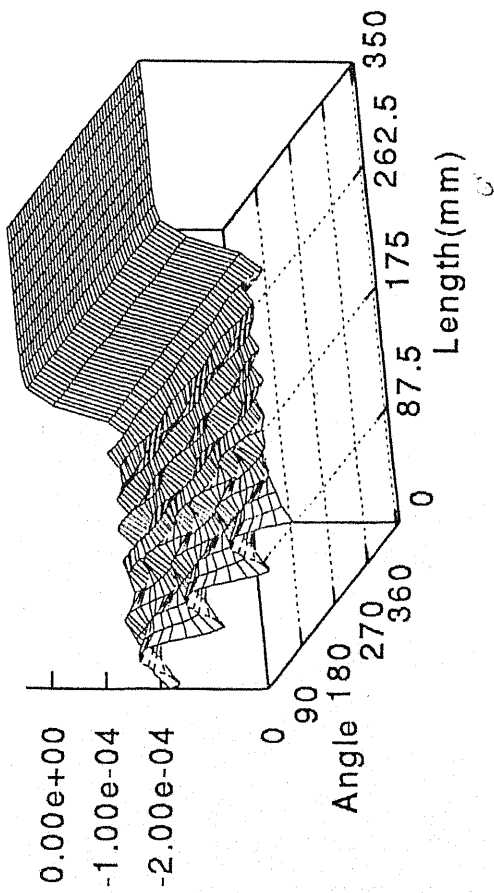
Time: 125 microsec
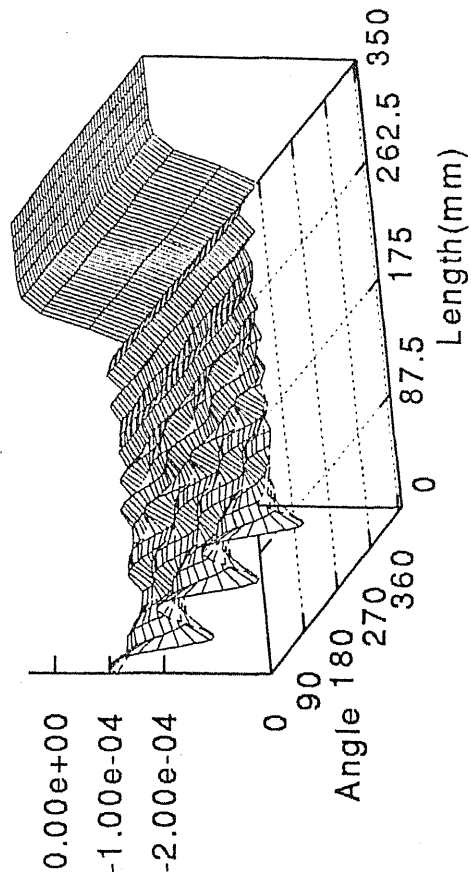
Disp

Time: 100 microsec

Disp

Time: 162.5 microsec
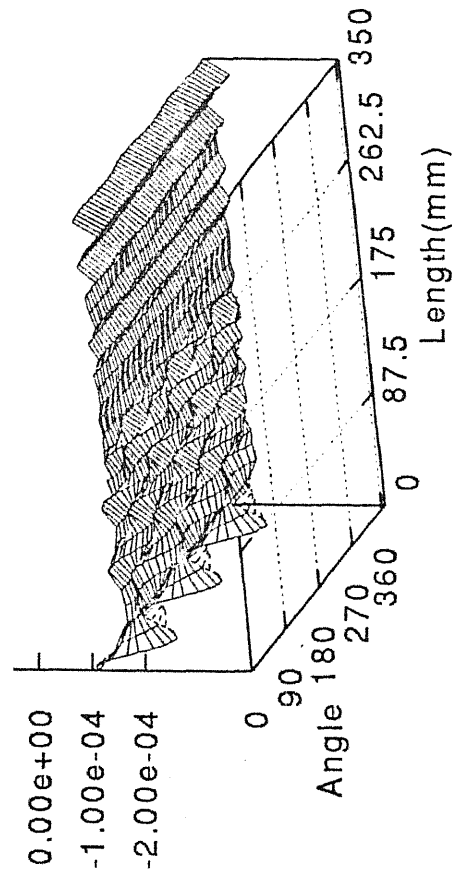
Disp

Time: 150 microsec

Disp

FIG 4.5(cont.): SNAPSHOTS OF CIRCUMFERENTIAL DISPLACEMENTS
DEFECT FREE SPECIMEN

44

FIG 4.5(cont.): SNAPSHOTS OF CIRCUMFERENTIAL DISPLACEMENTS

DEFECT FREE SPECIMEN

45

FIG 4.6: SNAPSHOTS OF AXIAL DISPLACEMENTS
DEFECT FREE SPECIMEN

46
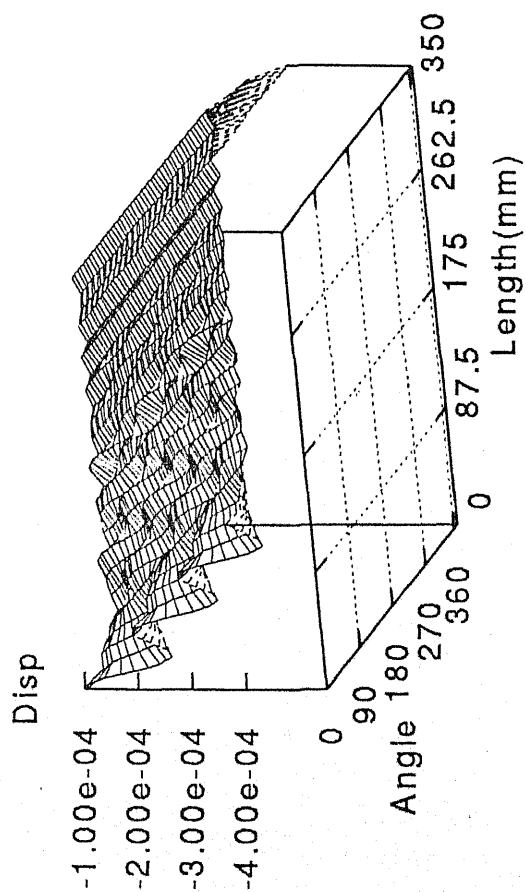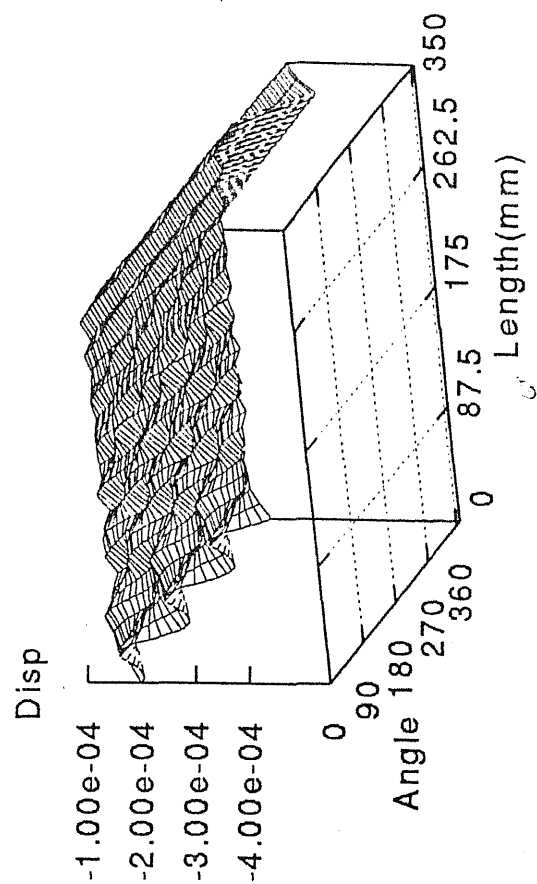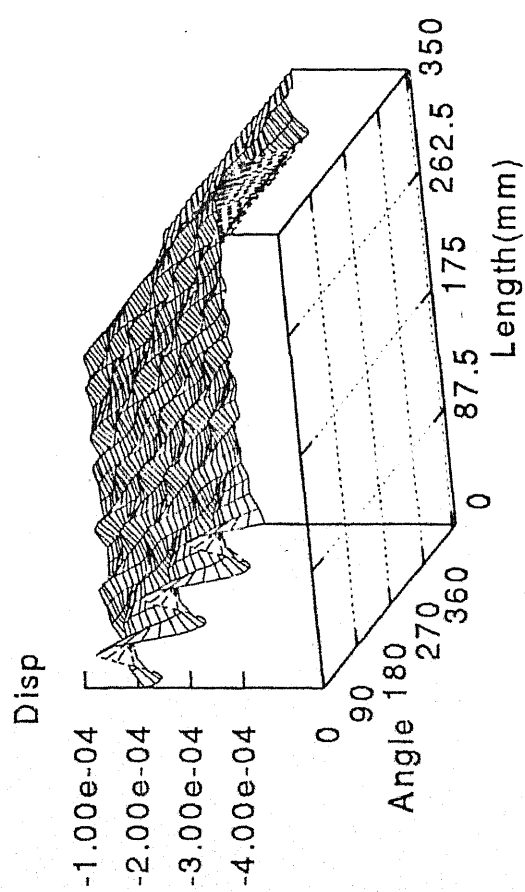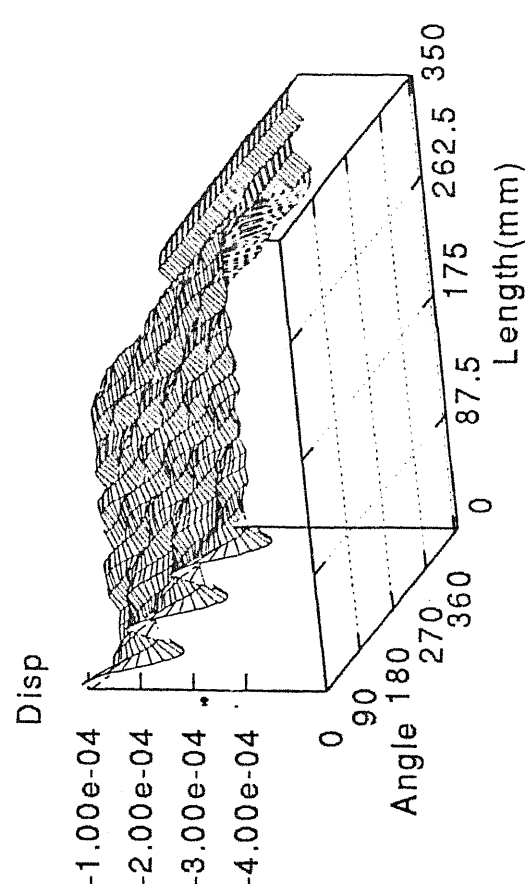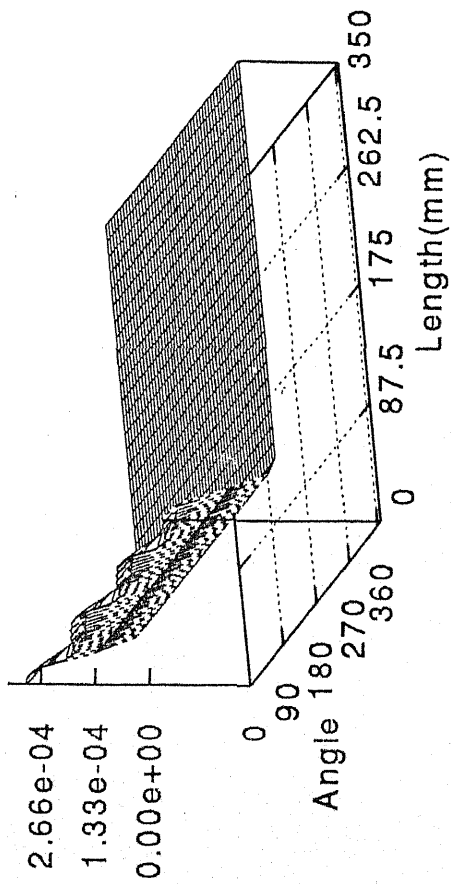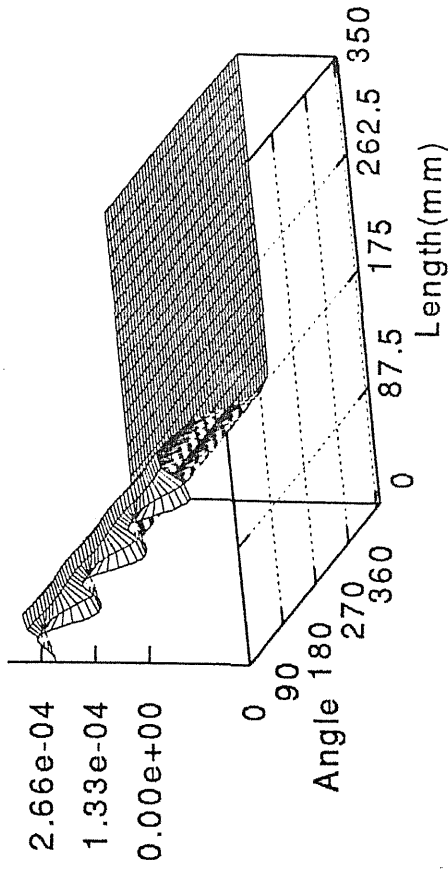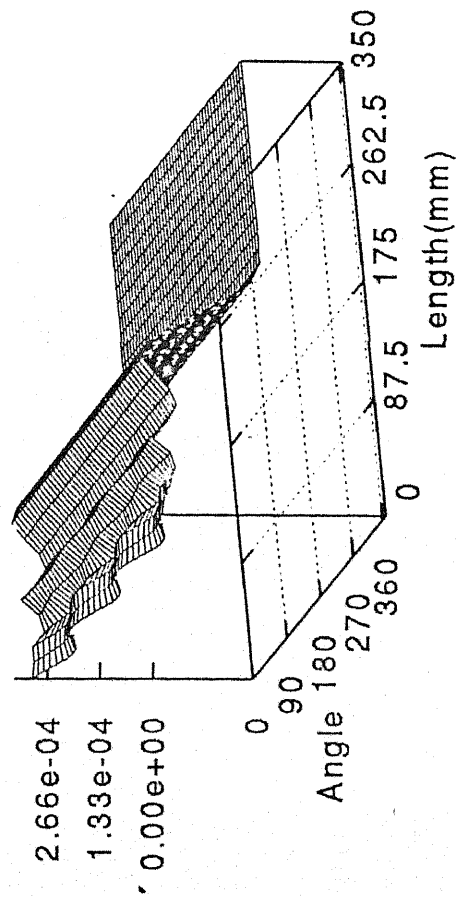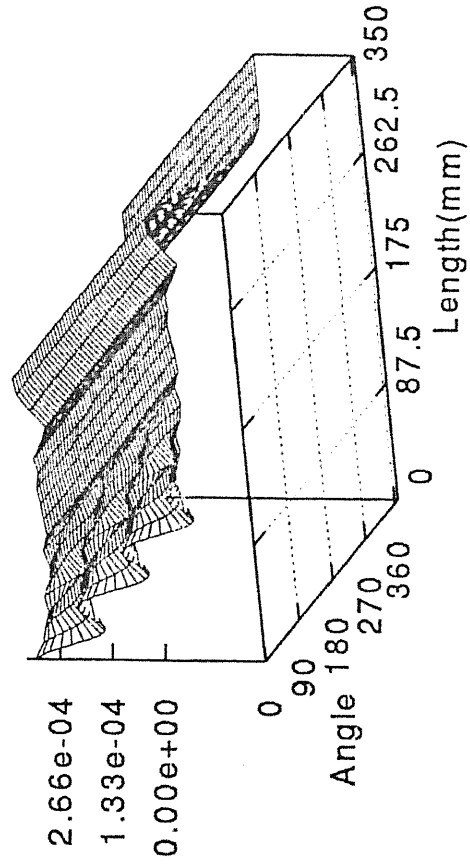
FIG 4.6(cont.): SNAPSHOTS OF AXIAL DISPLACEMENTS
DEFECT FREE SPECIMEN
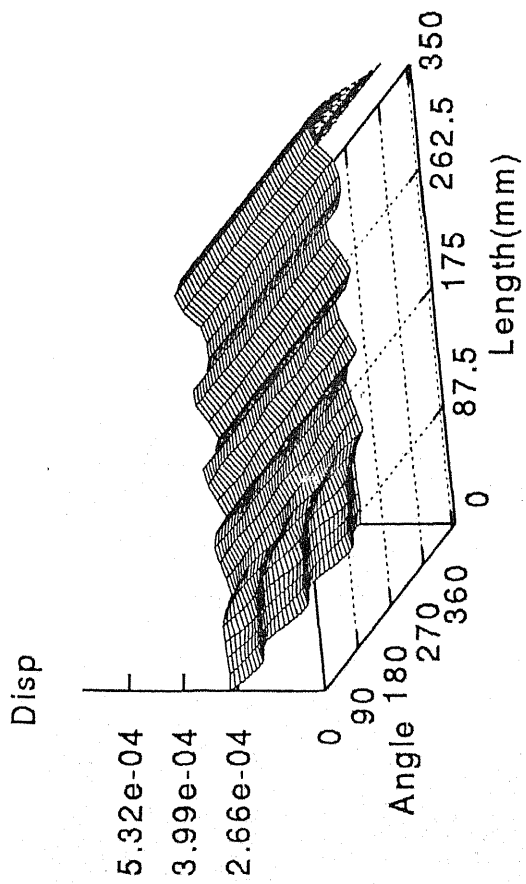
Time: 187.5 microsec

Time: 212.5 microsec

Time: 175 microsec

Time: 200 microsec

FIG 4.6(cont.): SNAPSHOTS OF AXIAL DISPLACEMENTS

DEFECT FREE SPECIMEN

48
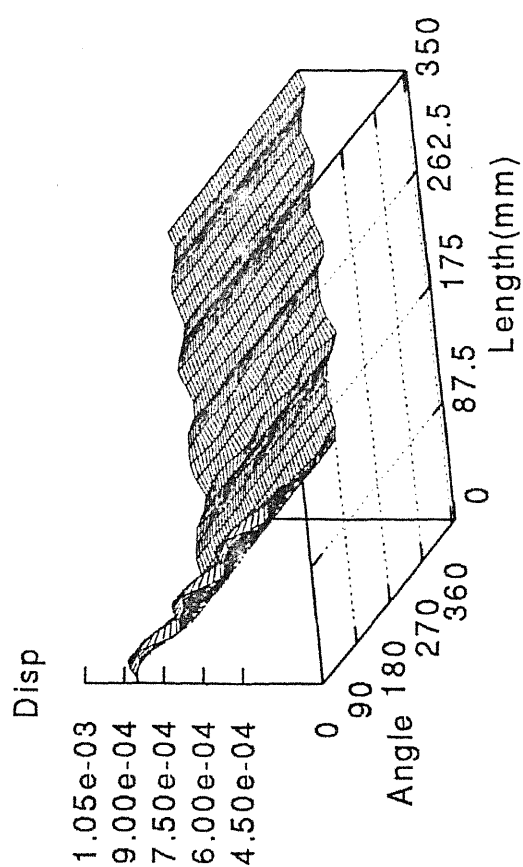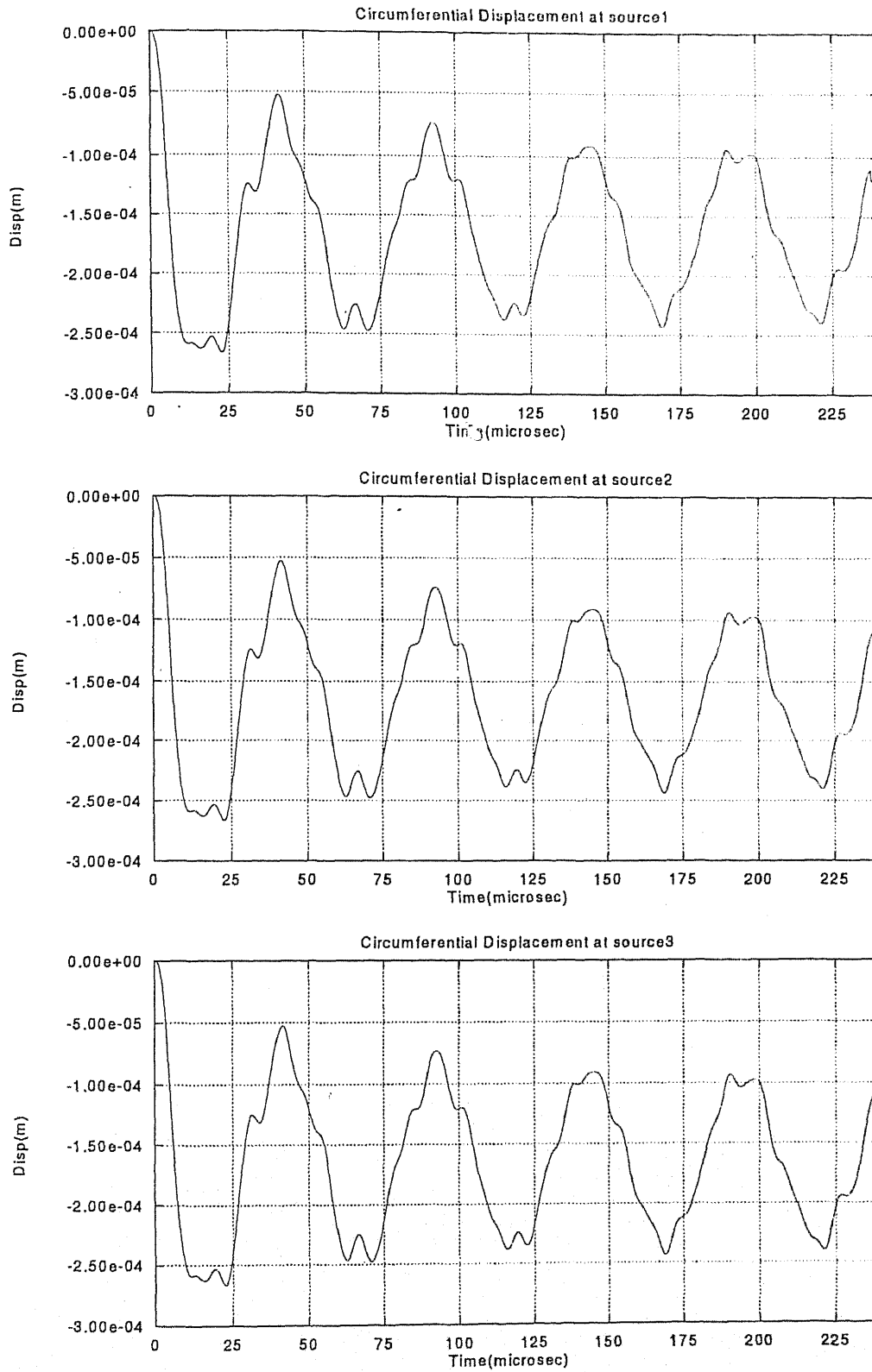
FIG 4.7: CIRCUMFERENTIAL DISPLACEMENTS AT THREE SOURCE LOCATIONS

DEFECT FREE SPECIMEN
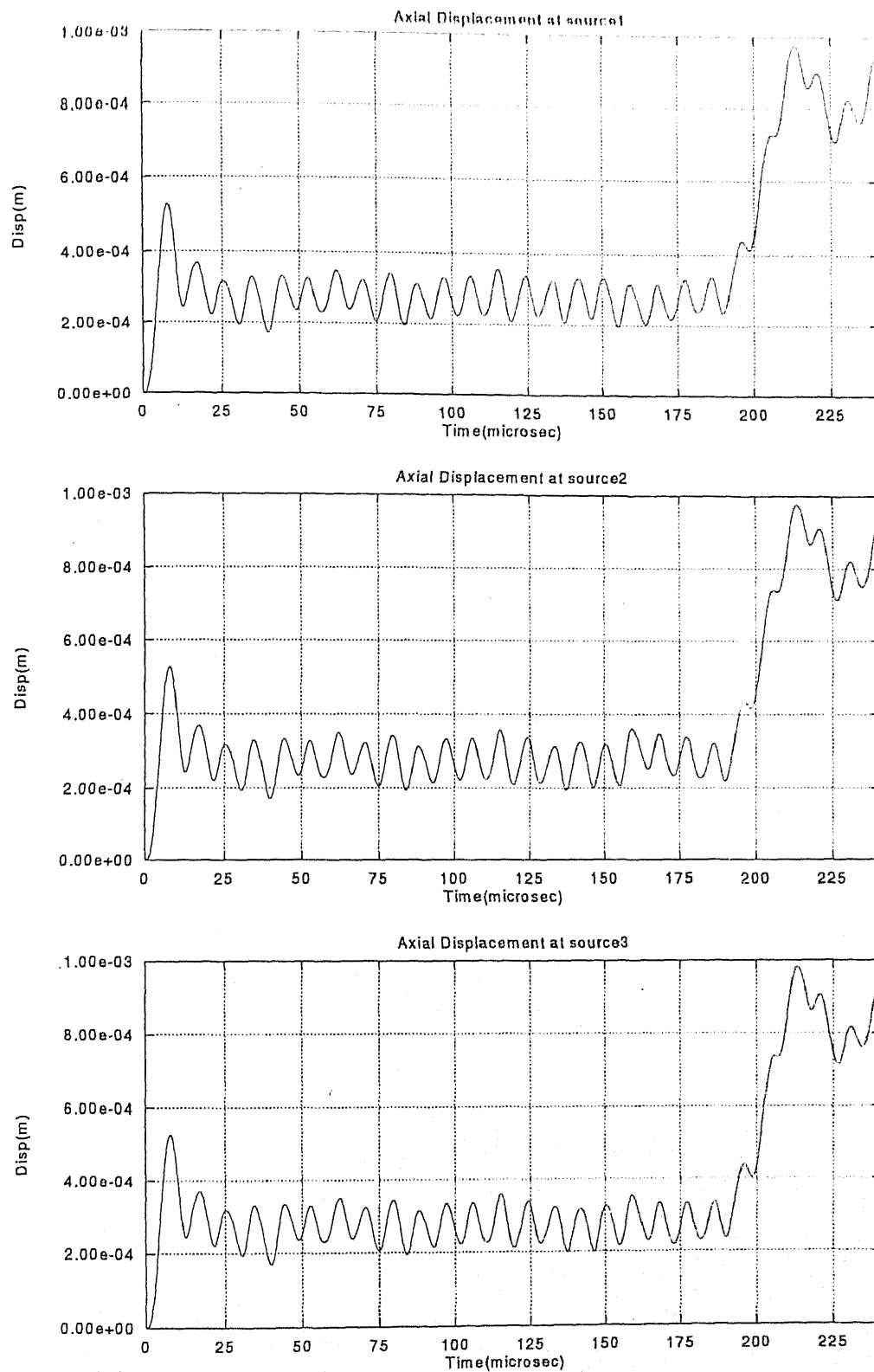
FIG 4.8: AXIAL DISPLACEMENTS AT THREE SOURCE LOCATIONS
DEFECT FREE SPECIMEN

FIG 4.9: SPECIMEN GEOMETRY AND LOADING
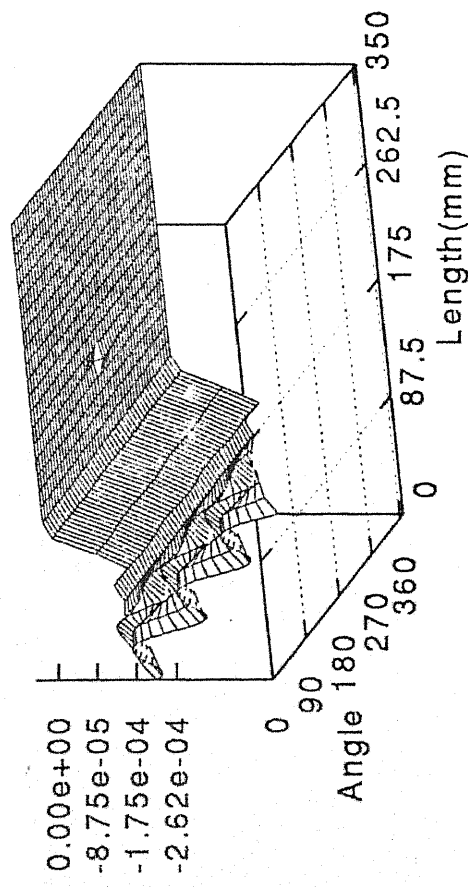CIRCUMFERENTIAL CRACK: L=175mm ,Θ=180 deg

Time: 12.5 microsec

Time: 25 microsec

Time: 50 microsec

Time: 75 microsec

FIG 4.10: SNAPSHOTS OF CIRCUMFERENTIAL DISPLACEMENTS
CIRCUMFERENTIAL CRACK: L=175mm, Θ=180 deg

52

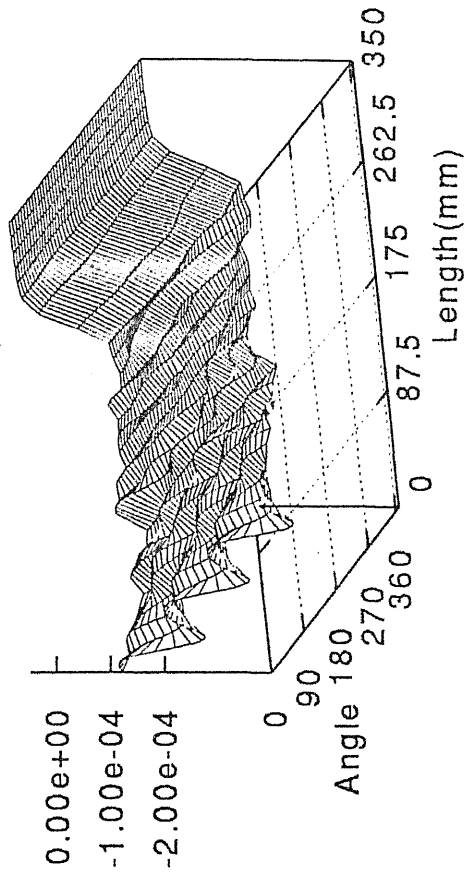FIG 4.10(cont.): SNAPSHOTS OF CIRCUMFERENTIAL DISPLACEMENTS
CIRCUMFERENTIAL CRACK: L=175mm ,Θ=180 deg

Time: 187.5 microsec

Time: 212.5 microsec

Time: 175 microsec

Time: 200 microsec
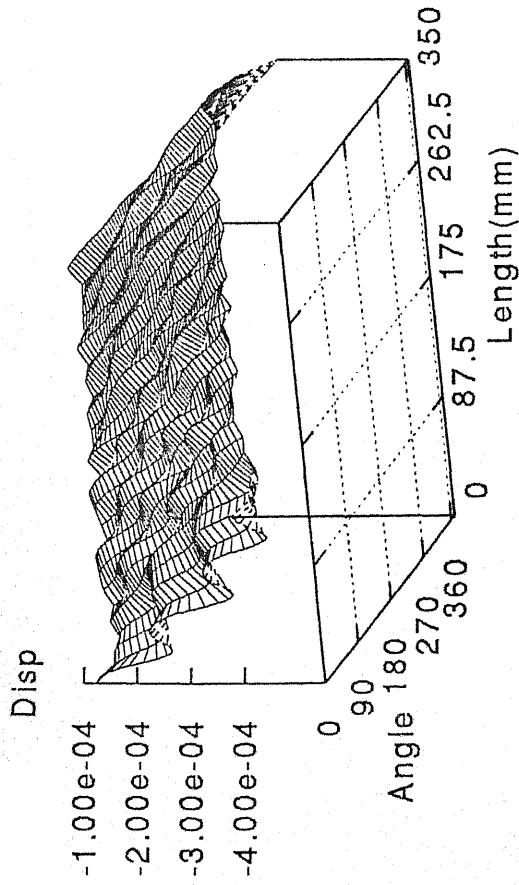
FIG 4.10(cont.): SNAPSHOTS OF CIRCUMFERENTIAL DISPLACEMENTS
CIRCUMFERENTIAL CRACK: L=175mm ,Θ=180 deg

54

Time: 25 microsec

Time: 12.5 microsec

Time: 75 microsec

Time: 50 microsec

FIG 4.11: SNAPSHOTS OF AXIAL DISPLACEMENTS
CIRCUMFERENTIAL CRACK: L=175mm, ⊖=180 deg

55

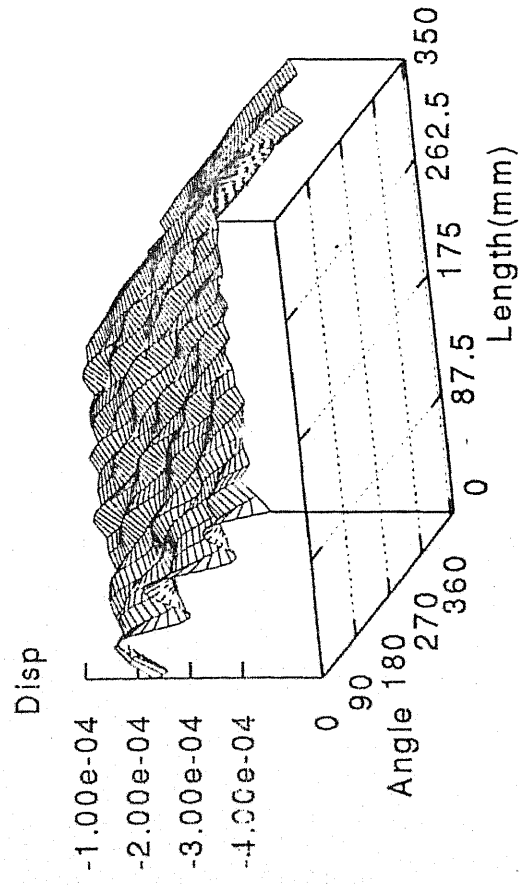FIG 4.11(cont.): SNAPSHOTS OF AXIAL DISPLACEMENTS
CIRCUMFERENTIAL CRACK: L=175mm, Θ=180 deg
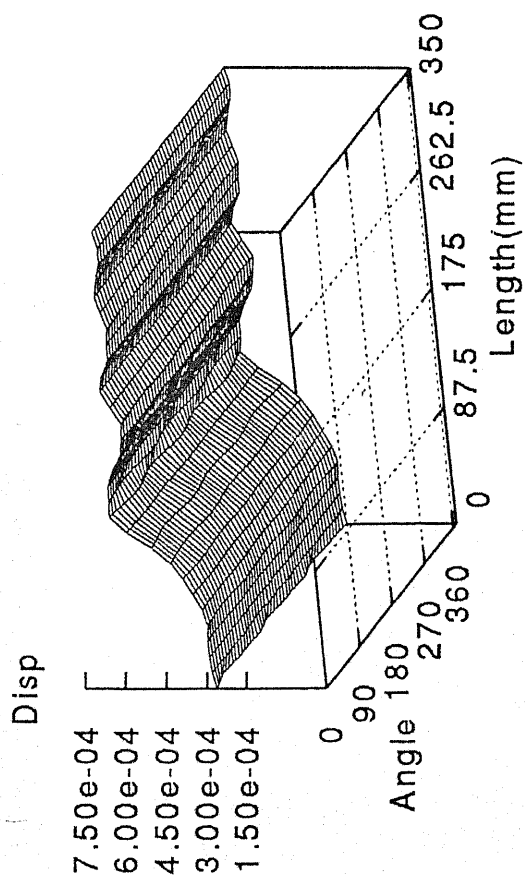
Time: 187.5 microsec
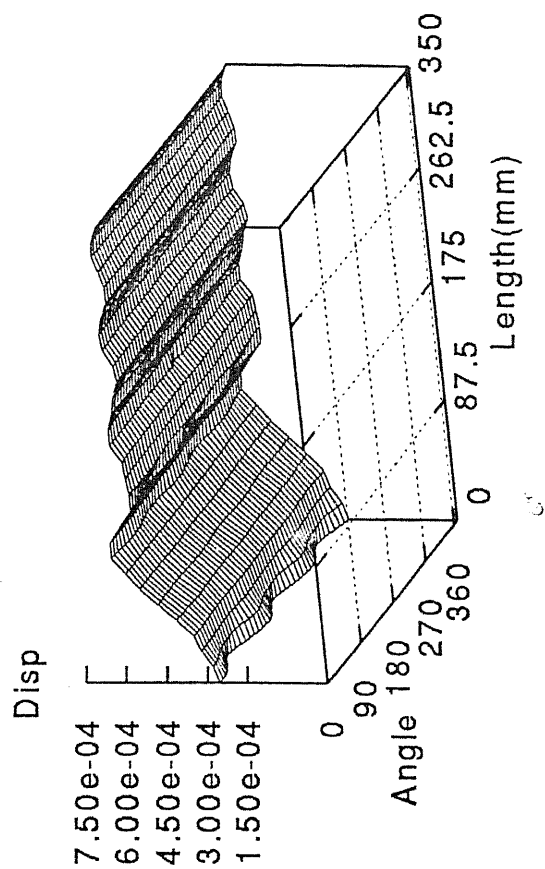
Time: 175 microsec
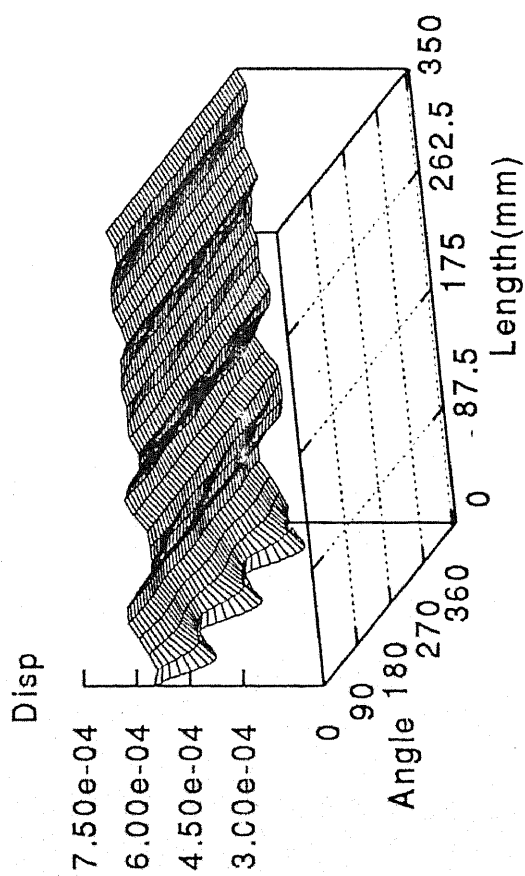
Time: 212.5 microsec

Time: 200 microsec

FIG 4.11(cont.): SNAPSHOTS OF AXIAL DISPLACEMENTS
CIRCUMFERENTIAL CRACK: L=175mm ,Θ=180 deg
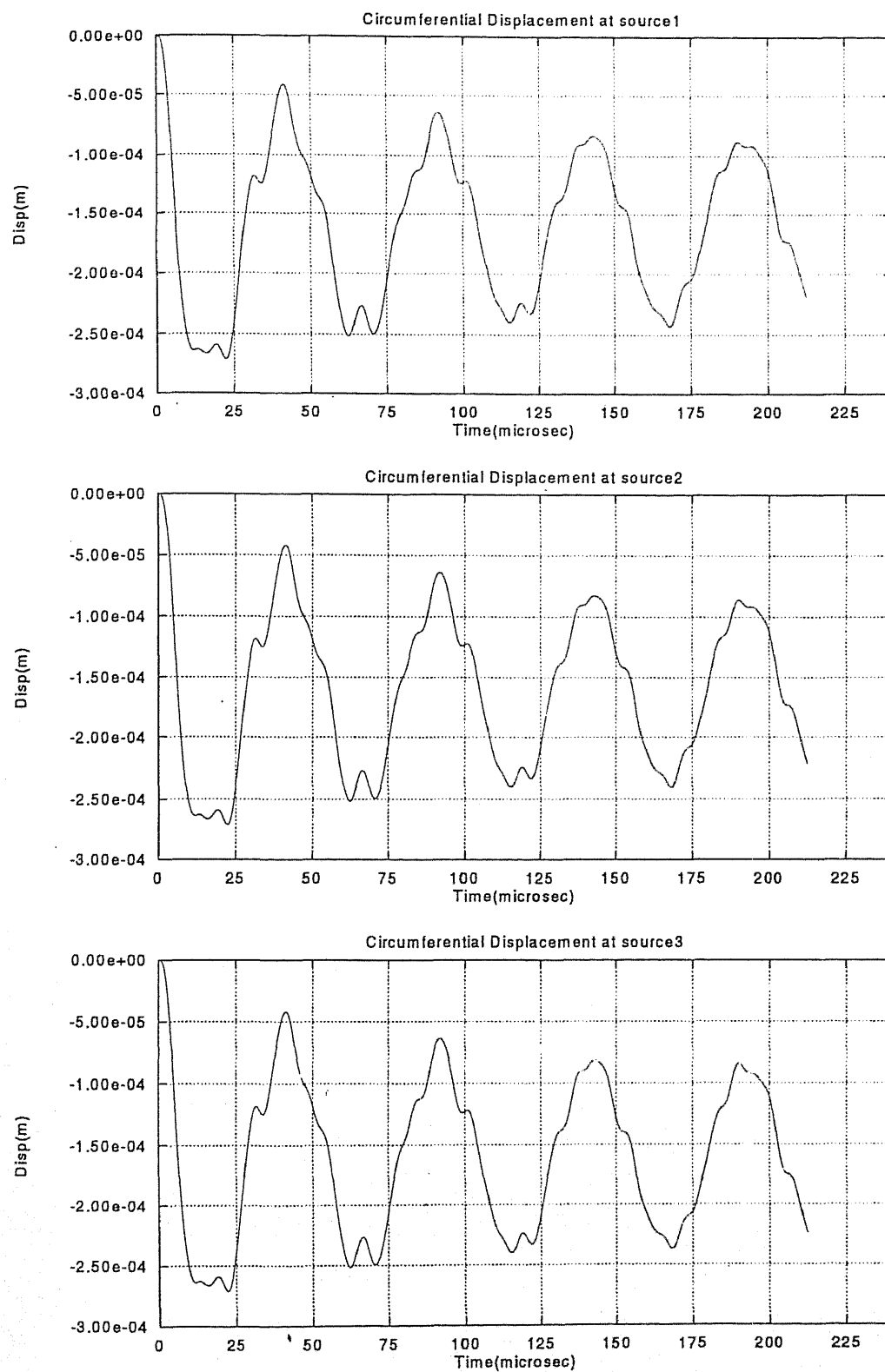
FIG 4.12: CIRCUMFERENTIAL DISPLACEMENTS AT THREE SOURCE LOCATIONS
CIRCUMFERENTIAL CRACK: L=175mm ,Θ=180 deg
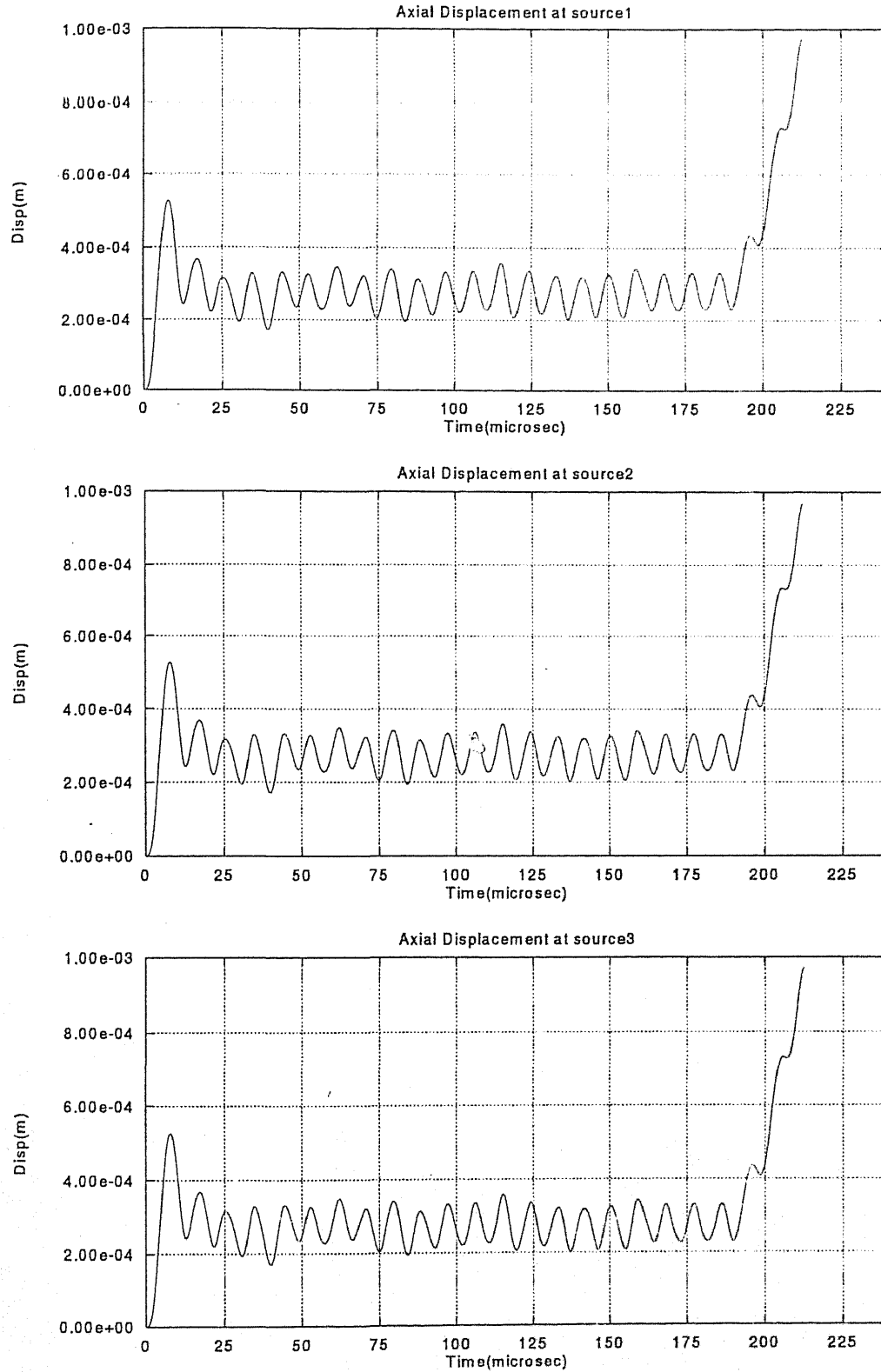
FIG 4.13: AXIAL DISPLACEMENTS AT THREE SOURCE LOCATIONS

CIRCUMFERENTIAL CRACK: L=175mm ,Θ=180 deg
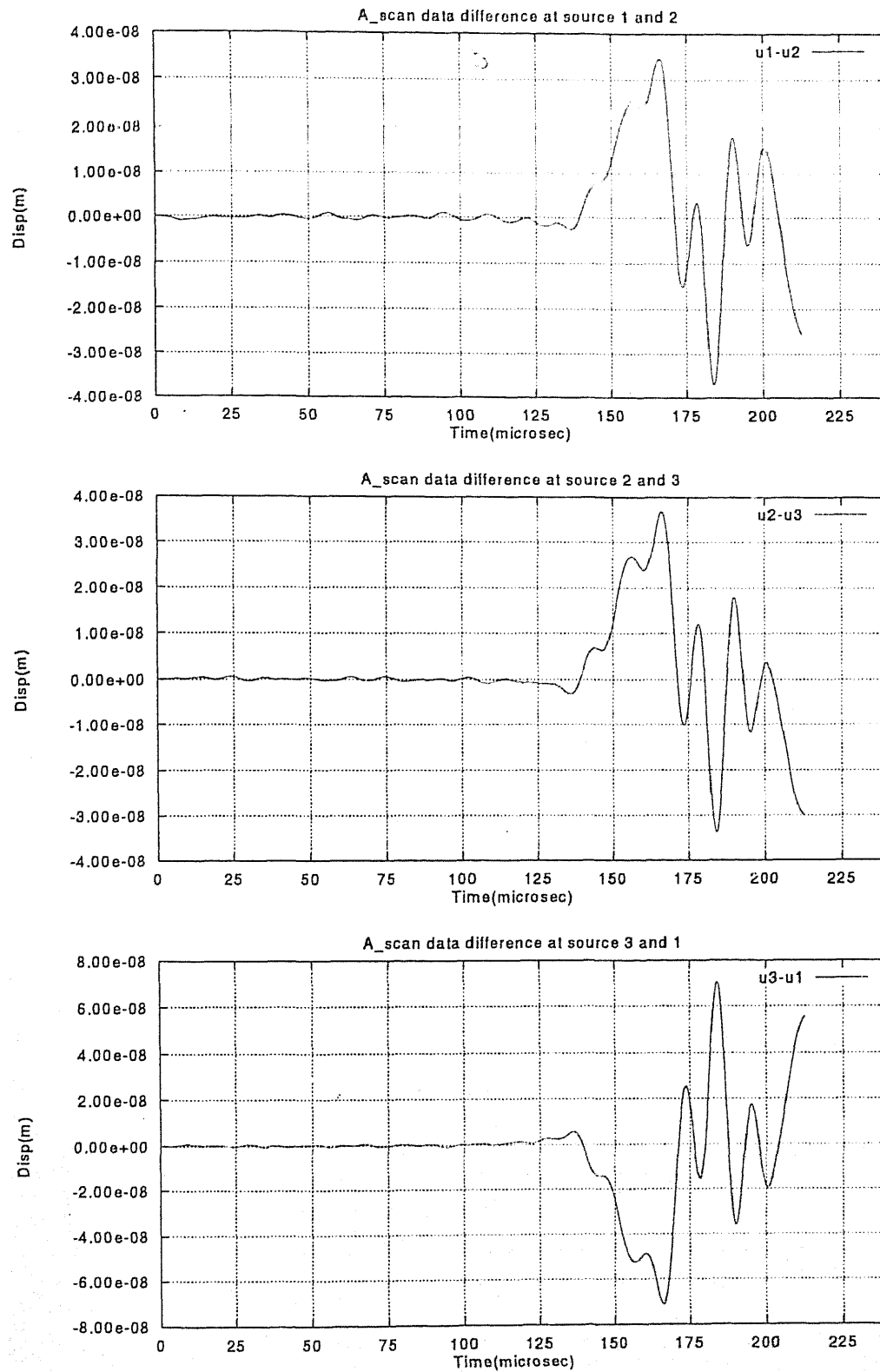
FIG 4.14: A-SCAN PLOTS OF DIFFERENCE OF CIRCUMFERENTIAL DISPLACEMENT
AT THE SOURCE LOCATIONS
CIRCUMFERENTIAL CRACK: L=175mm ,Θ=180 deg

FIG 4.15: A-SCAN PLOTS OF DIFFERENCE OF CIRCUMFERENTIAL DISPLACEMENT
AT THE SOURCE LOCATIONS

FIG 4.16: SPECIMEN GEOMETRY AND LOADING
CIRCUMFERENTIAL CRACK: L=233.3mm, Θ=225 deg

FIG 4.17: SNAPSHOTS OF CIRCUMFERENTIAL DISPLACEMENTS
CIRCUMFERENTIAL CRACK: L=233.3mm, Θ=225 deg

63

FIG 4.17(cont.): SNAPSHOTS OF CIRCUMFERENTIAL DISPLACEMENTS
CIRCUMFERENTIAL CRACK: L=233.3mm, Θ=225 deg

64

Time: 175 microsec

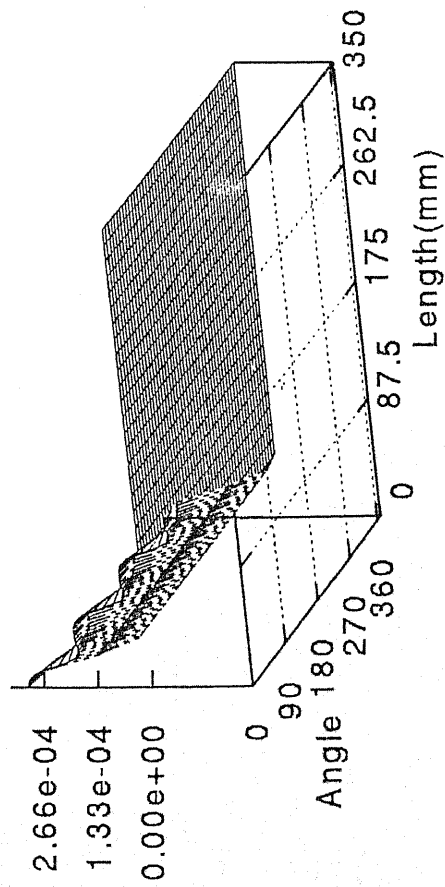Time: 187.5 microsec

Time: 200 microsec

Time: 212.5 microsec

FIG 4.17(cont.): SNAPSHOTS OF CIRCUMFERENTIAL DISPLACEMENTS
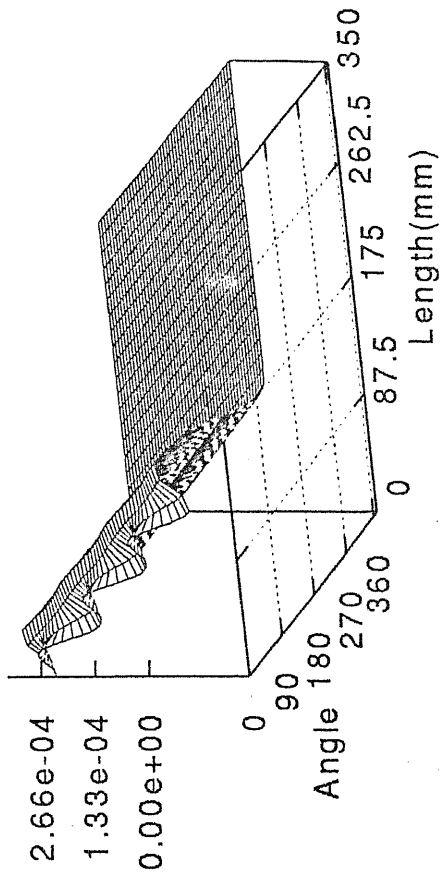
CIRCUMFERENTIAL CRACK: L=233.3mm, Θ=225 deg

FIG 4.18: SNAPSHOTS OF AXIAL DISPLACEMENTS
CIRCUMFERENTIAL CRACK: L=233.3mm, Θ=225 deg

66

Time: 125 microsec

Disp

5.32e-04
3.99e-04
2.66e-04

Angle 180

270
360

0
90

0
87.5
175
262.5
350
Length(mm)

Time: 162.5 microsec

Disp

5.32e-04
3.99e-04
2.66e-04

Angle 180

270
360

0
90

0
87.5
175
262.5
350
Length(m)

Time: 100 microsec

Disp

5.32e-04
3.99e-04
2.66e-04

Angle 180

270
360

0
90

0
87.5
175
262.5
350
Length(mm)

Time: 150 microsec

Disp

5.32e-04
3.99e-04
2.66e-04

Angle 180

270
360

0
90

0
87.5
175
262.5
350
Length(mm)

FIG 4.18(cont.): SNAPSHOTS OF AXIAL DISPLACEMENTS
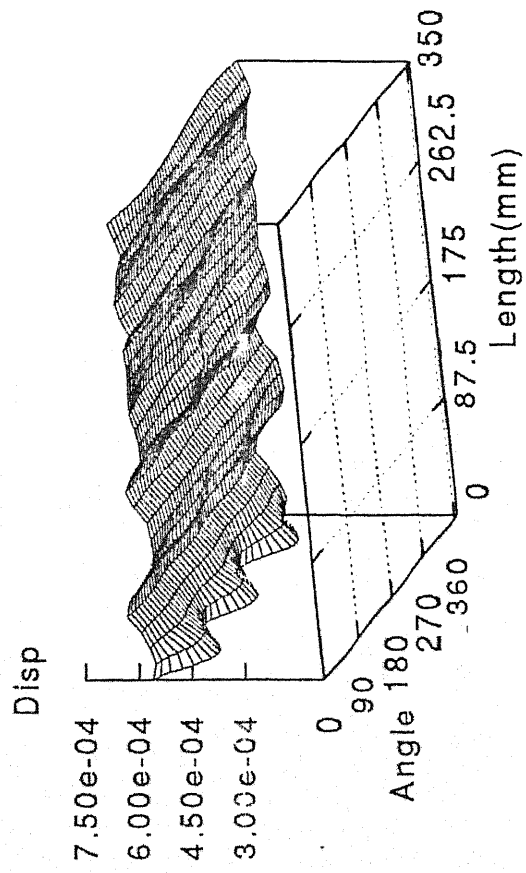
CIRCUMFERENTIAL CRACK: L=233.3mm, Θ=225 deg

Time: 175 microsec

Time: 187.5 microsec

Time: 200 microsec

Time: 212.5 microsec

FIG 4.18(cont.): SNAPSHOTS OF AXIAL DISPLACEMENTS
CIRCUMFERENTIAL CRACK: L=233.3mm, Θ=225 deg

FIG 4.19: CIRCUMFERENTIAL DISPLACEMENTS AT THREE SOURCE LOCATIONS
CIRCUMFERENTIAL CRACK: L=233.3mm, Θ=225 deg

FIG 4.20: AXIAL DISPLACEMENTS AT THREE SOURCE LOCATIONS

CIRCUMFERENTIAL CRACK: L=233.3mm, Θ=225 deg
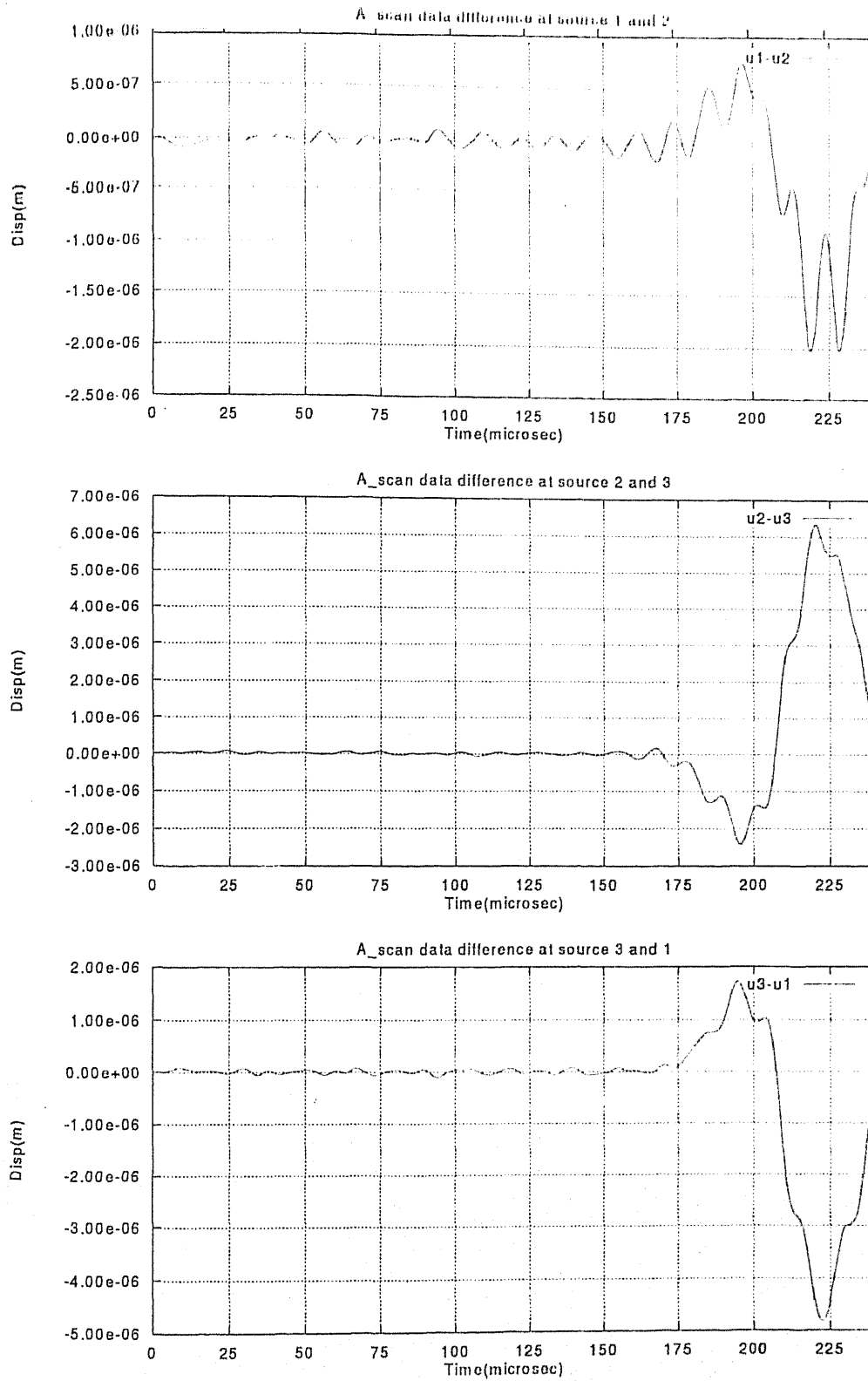
FIG 4.21: A-SCAN PLOTS OF DIFFERENCE OF CIRCUMFERENTIAL DISPLACEMENT
AT THE SOURCE LOCATIONS

CIRCUMFERENTIAL CRACK: L 233.3mm. Θ 225 deg

FIG 4.22: A-SCAN PLOTS OF DIFFERENCE OF CIRCUMFERENTIAL DISPLACEMENT
AT THE SOURCE LOCATIONS

FIG 4.23: SPECIMEN GEOMETRY AND LOADING
AXIAL CRACK: L 175mm, Θ 180 deg

FIG 4.24: SNAPSHOTS OF CIRCUMFERENTIAL DISPLACEMENTS

AXIAL CRACK: L=175mm, Θ=180 deg

74

Time: 125 microsec

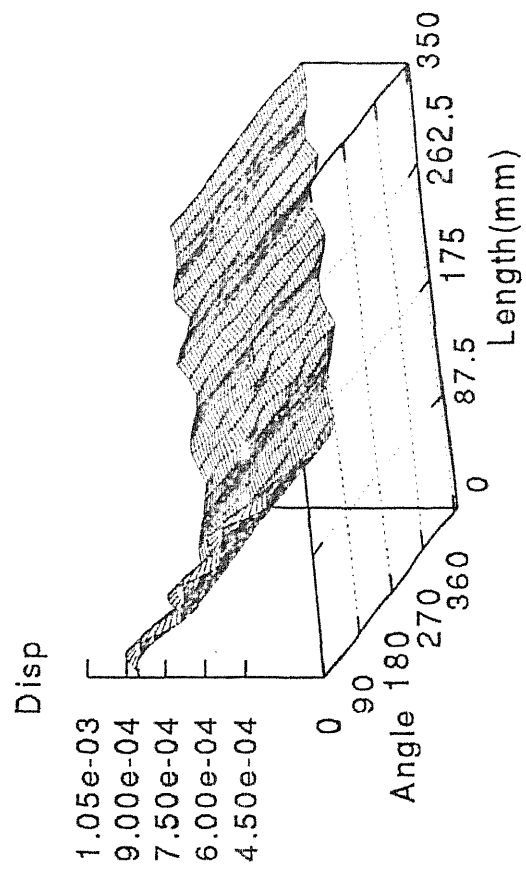Time: 100 microsec

Time: 162.5 microsec

Time: 150 microsec

FIG 4.24(cont.): SNAPSHOTS OF CIRCUMFERENTIAL DISPLACEMENTS
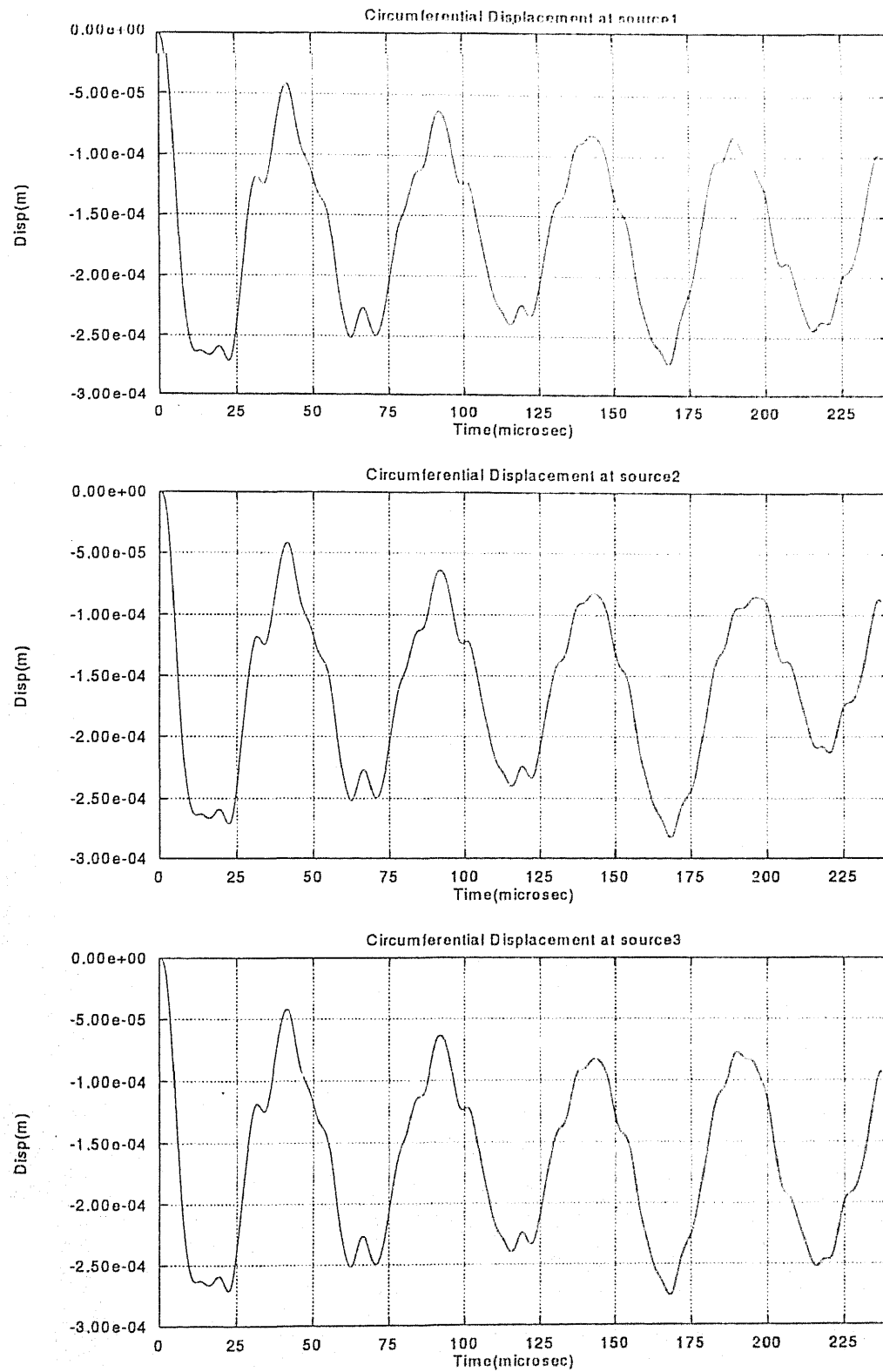AXIAL CRACK: L=175mm, Θ=180 deg

Time: 187.5 microsec

Time: 212.5 microsec

Time: 175 microsec

Time: 200 microsec

FIG 4.24(cont.): SNAPSHOTS OF CIRCUMFERENTIAL DISPLACEMENTS

AXIAL CRACK: L=175mm, Θ=180 deg

76

FIG 4.25: SNAPSHOTS OF AXIAL DISPLACEMENTS

AXIAL CRACK: L=175mm, Θ=180 deg

77

Time: 125 microsec

Disp

5.32e-04
3.99e-04
2.66e-04

0

Angle 180
270
360
90
0

87.5   175   262.5   350
Length(mm)

Time: 162.5 microsec

Disp

5.32e-04
3.99e-04
2.66e-04

0

Angle 180
270
360
90
0

87.5   175   262.5   350
Length(mm)

Time: 100 microsec

Disp

5.32e-04
3.99e-04
2.66e-04

0

Angle 180
270
360
90
0

87.5   175   262.5   350
Length(mm)

Time: 150 microsec

Disp

5.32e-04
3.99e-04
2.66e-04

0

Angle 180
270
360
90
0

87.5   175   262.5   350
Length(mm)

FIG 4.25(cont.): SNAPSHOTS OF AXIAL DISPLACEMENTS
AXIAL CRACK: L=175mm, Θ=180 deg

FIG 4.25(cont.): SNAPSHOTS OF AXIAL DISPLACEMENTS

AXIAL CRACK: L=175mm, Θ=180 deg

FIG 4.26: CIRFERENTIAL DISPLACEMENTS AT THREE SOURCE LOCATIONS
AXIAL CRACK: L=175mm, Θ=180 deg

FIG 4.27: AXIAL DISPLACEMENTS AT THREE SOURCE LOCATIONS
AXIAL CRACK: L=175mm, Θ=180 deg

FIG 4.28: A-SCAN PLOTS OF DIFFERENCE OF CIRCUMFERENTIAL DISPLACEMENT
AT THE SOURCE LOCATIONS
AXIAL CRACK: L=175mm, Θ=180 deg
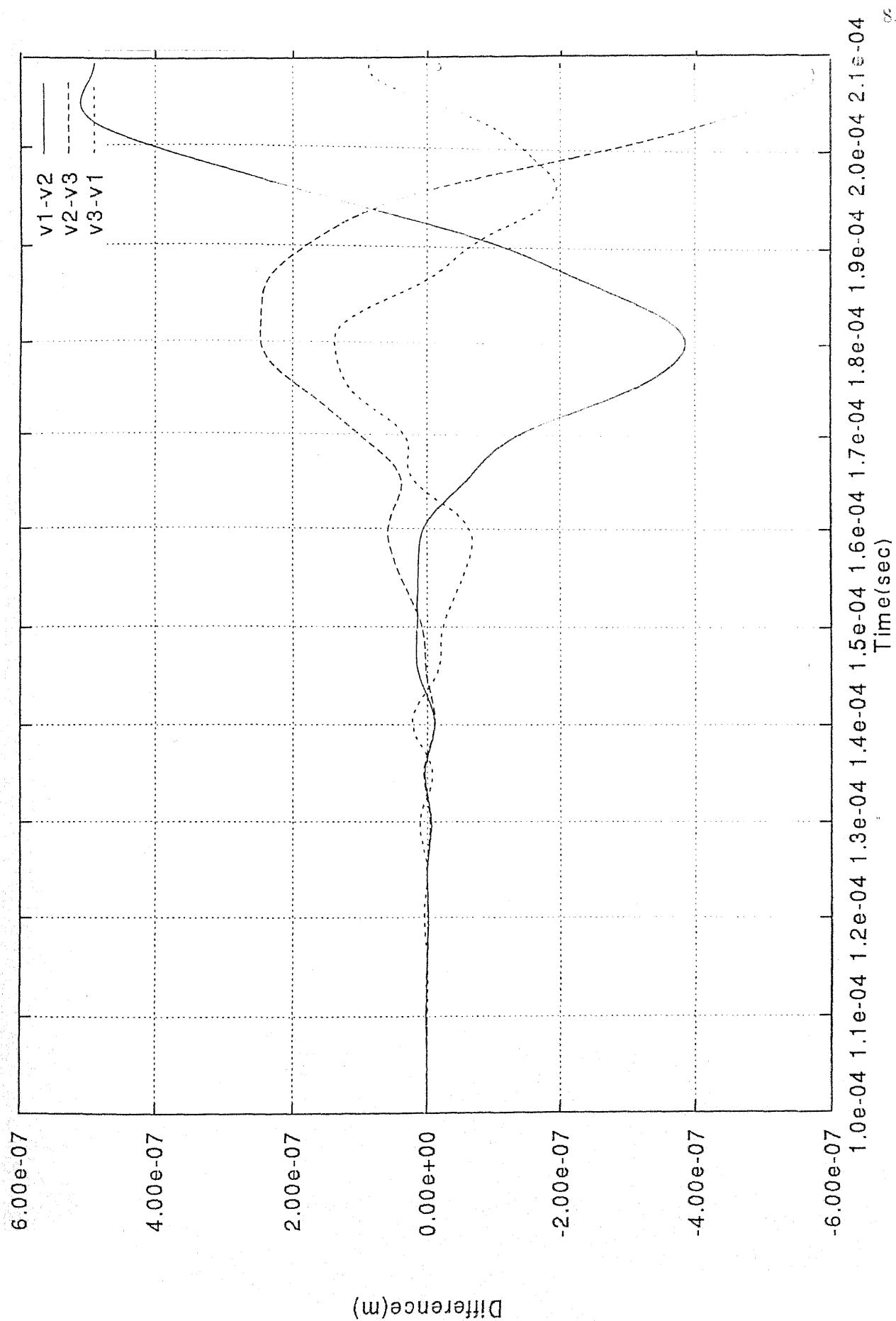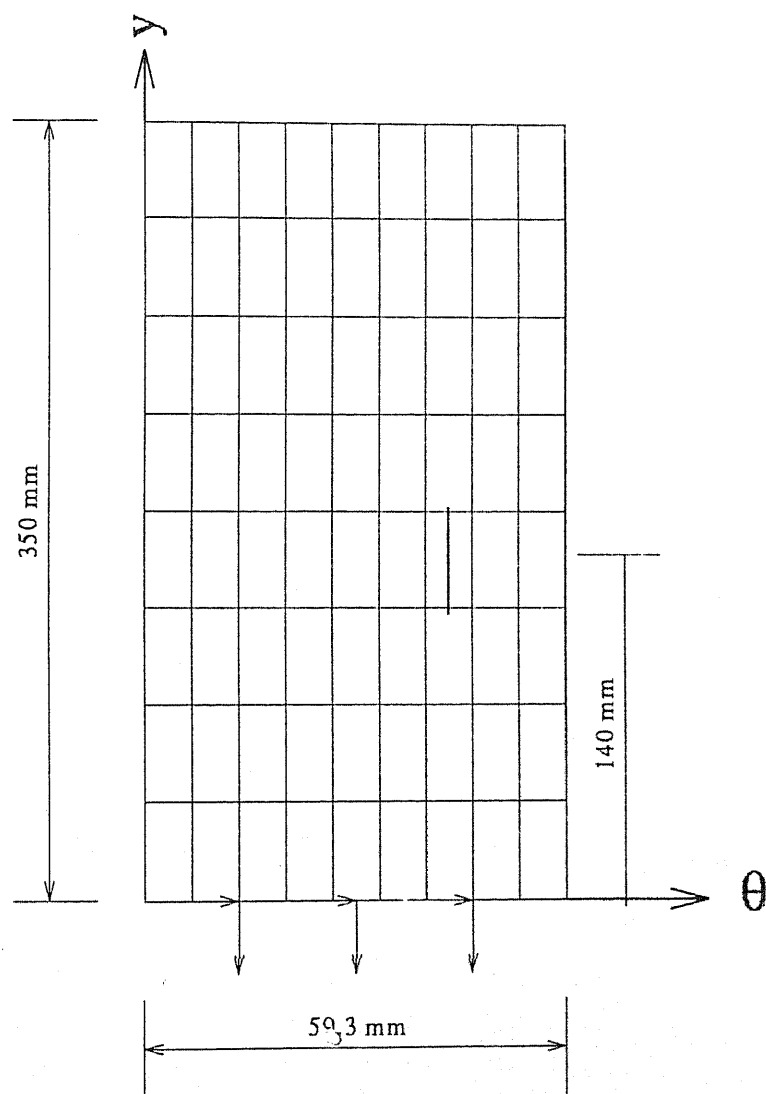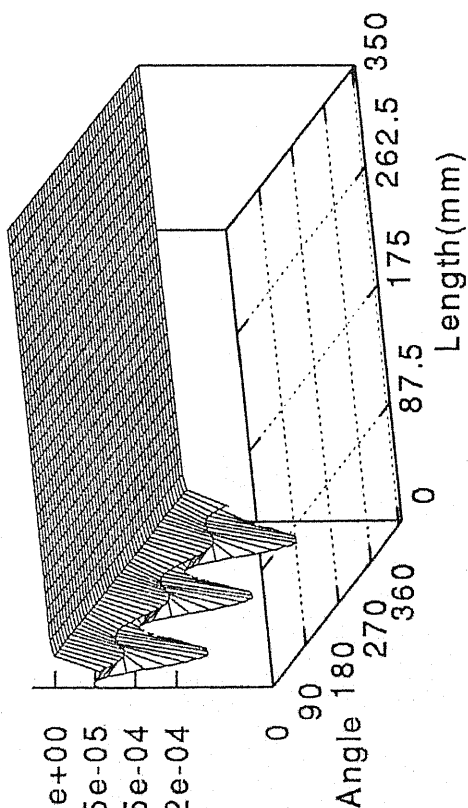
FIG 4.29. A-SCAN PLOTS OF DIFFERENCE OF CIRCUMFERENTIAL DISPLACEMENT
AT THE SOURCE LOCATIONS

FIG 4.30: SPECIMEN GEOMETRY AND LOADING
AXIAL CRACK: L 140mm, θ 120 deg.
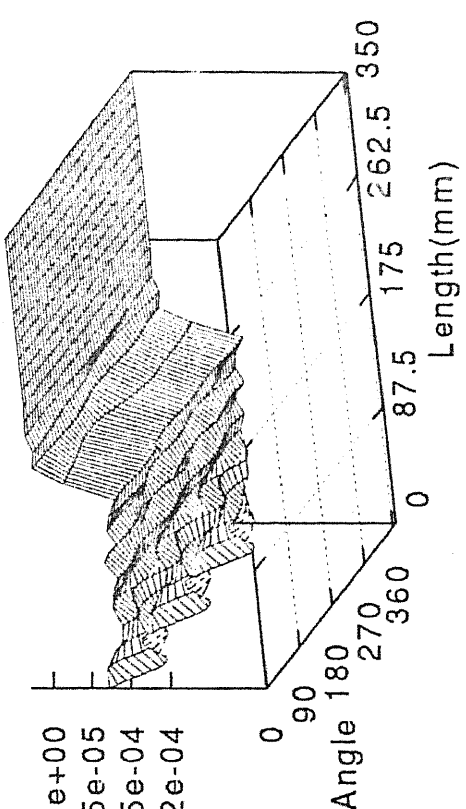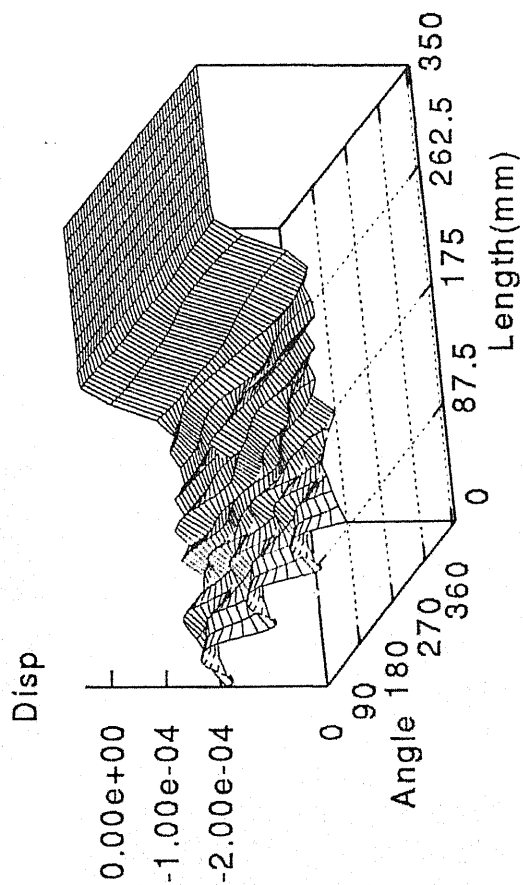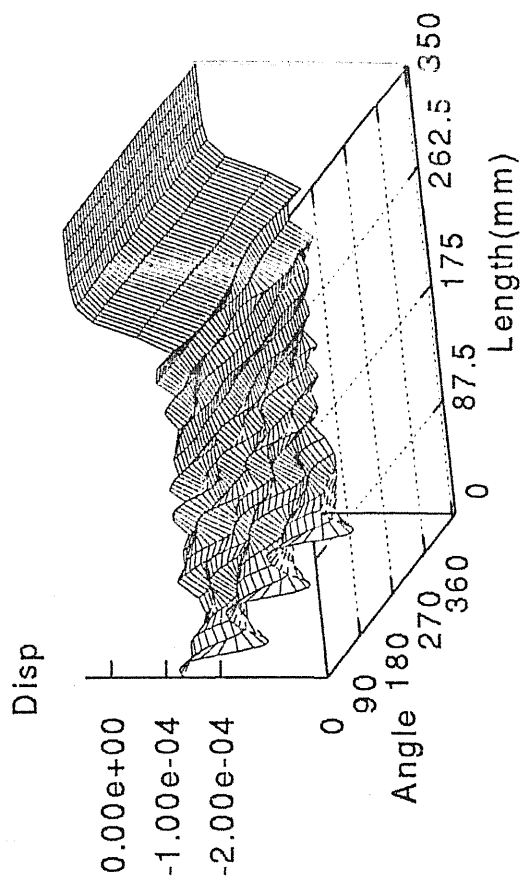
FIG 4.31: SNAPSHOTS OF CIRCUMFERENTIAL DISPLACEMENTS
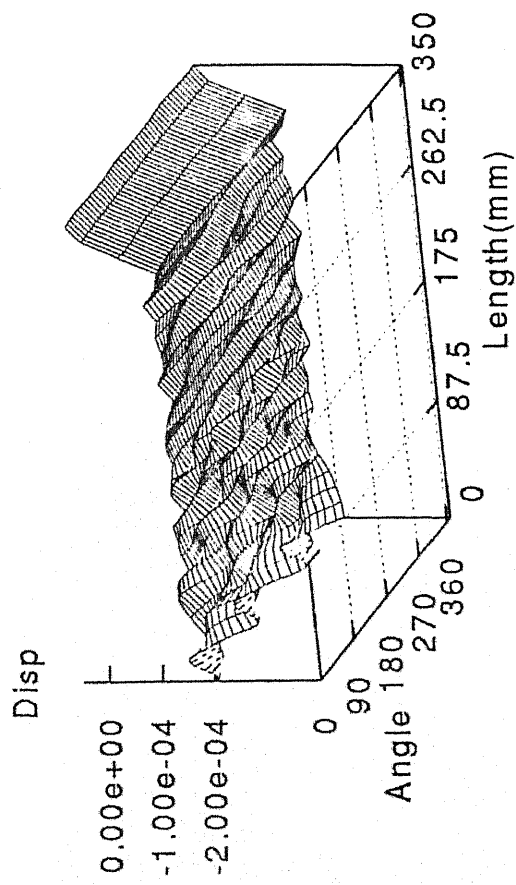AXIAL CRACK: L=140mm, Θ=120 deg

Time: 125 microsec

Time: 162.5 microsec

Time: 100 microsec

Time: 150 microsec

FIG 4.31(cont.): SNAPSHOTS OF CIRCUMFERENTIAL DISPLACEMENTS
AXIAL CRACK: L=140mm. Θ=120 deg

86

Time: 187.5 microsec
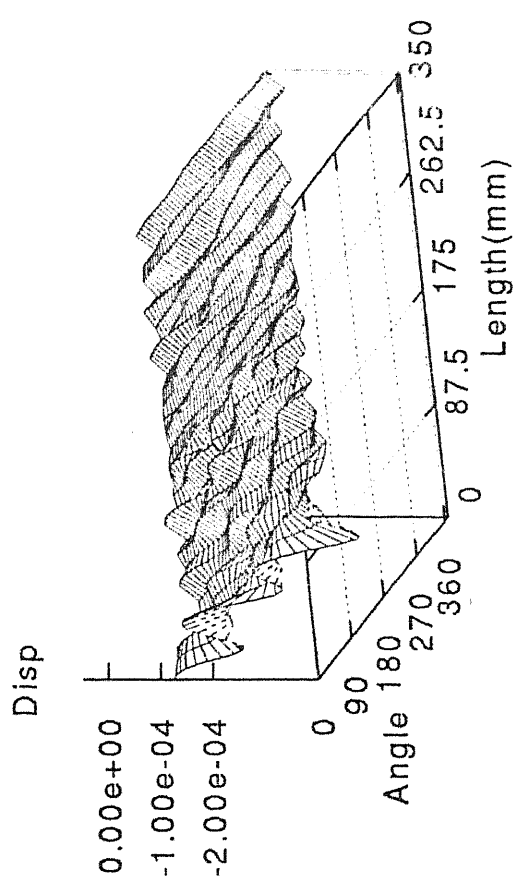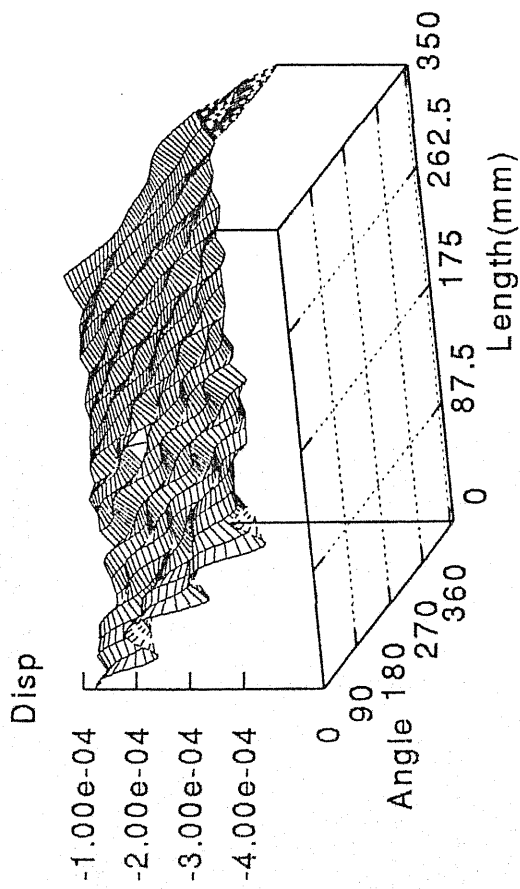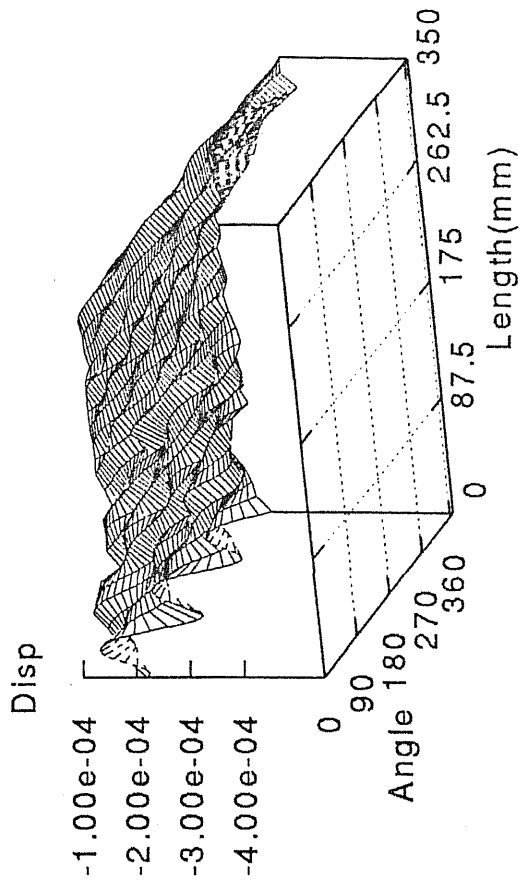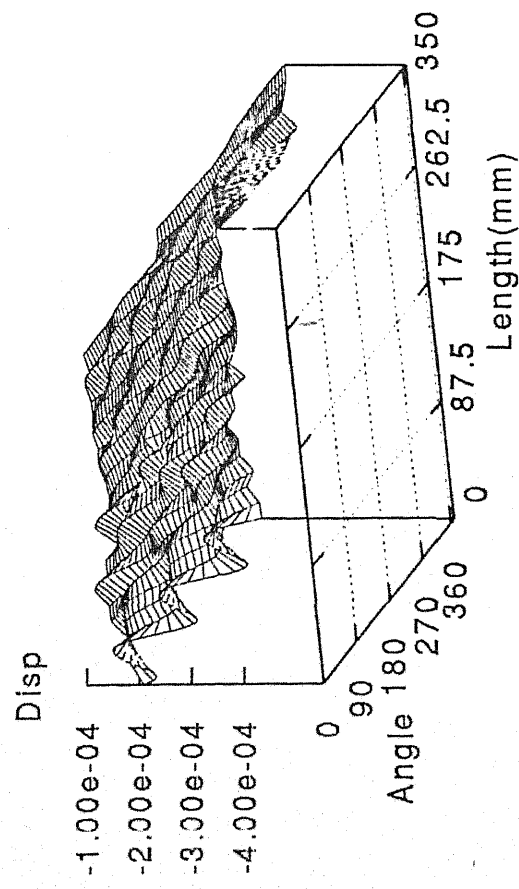
Time: 175 microsec

Time: 212.5 microsec

Time: 200 microsec

FIG 4.31(cont.): SNAPSHOTS OF CIRCUMFERENTIAL DISPLACEMENTS

AXIAL CRACK: L=140mm, Θ=120 deg

FIG 4.32: SNAPSHOTS OF AXIAL DISPLACEMENTS

AXIAL CRACK: L=140mm, Θ=120 deg

Time: 125 microsec
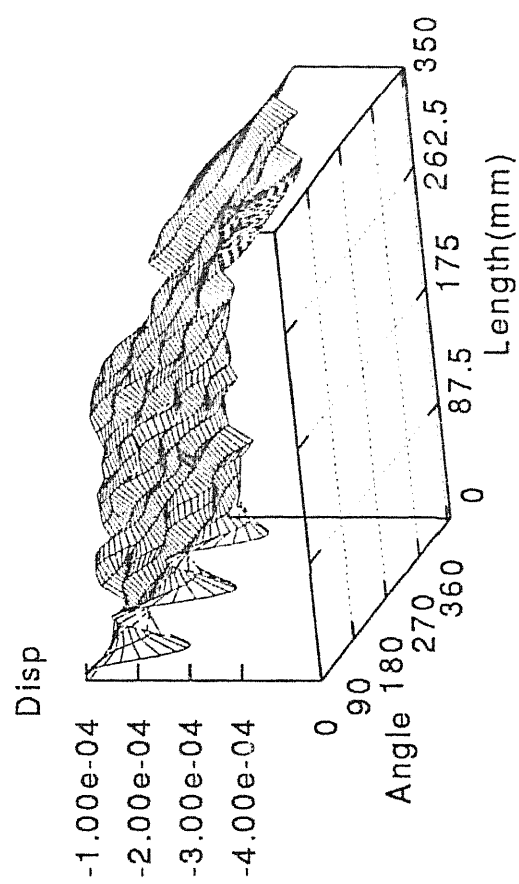
Time: 162.5 microsec

Time: 100 microsec

Time: 150 microsec

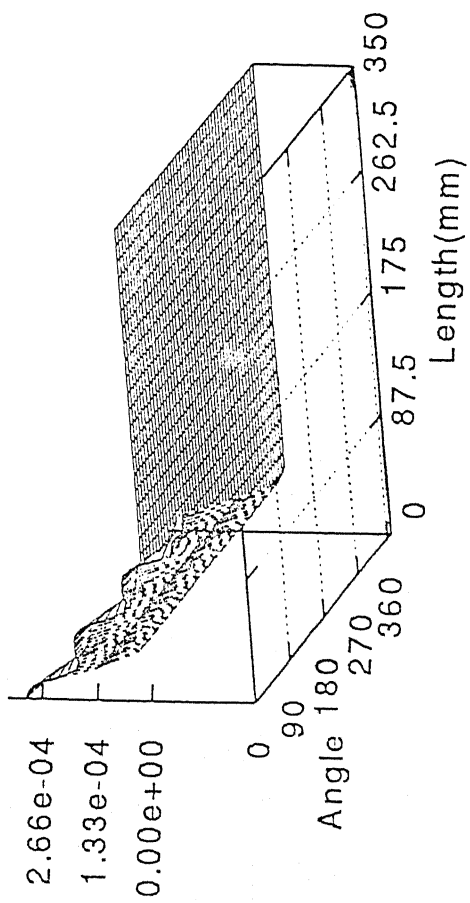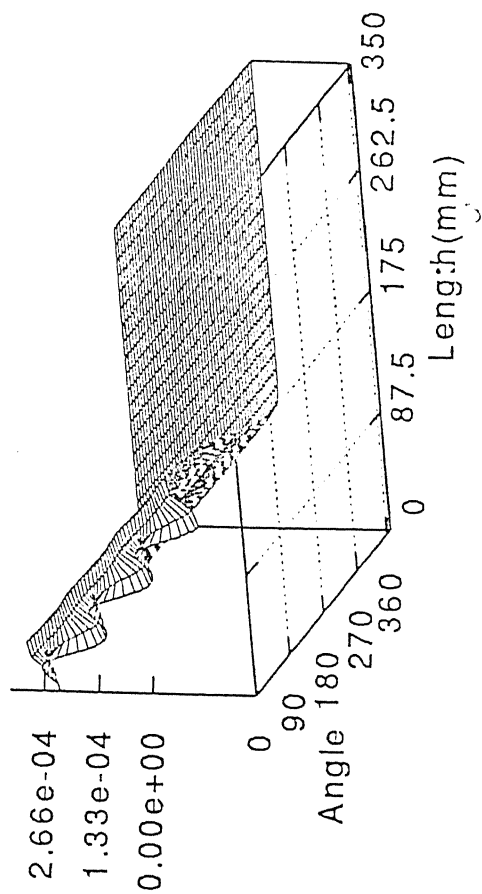FIG 4.32(cont.): SNAPSHOTS OF AXIAL DISPLACEMENTS

AXIAL CRACK. L=140mm, Θ=120 deg

Time: 175 microsec

Disp

7.50e-04
6.00e-04
4.50e-04
3.00e-04
1.50e-04

Angle 180
90
0
270
360

0
87.5
175
262.5
350

Length(mm)

Time: 187.5 microsec

Disp

7.50e-04
6.00e-04
4.50e-04
3.00e-04
1.50e-04

Angle 180
90
0
270
360

0
87.5
175
262.5
350

Length(mm)

Time: 200 microsec

Disp

7.50e-04
6.00e-04
4.50e-04
3.00e-04

Angle 180
90
0
270
360

0
87.5
175
262.5
350

Length(mm)

Time: 212.5 microsec

Disp

1.05e-03
9.00e-04
7.50e-04
6.00e-04
4.50e-04

Angle 180
90
0
270
360

0
87.5
175
262.5
350

Length(mm)
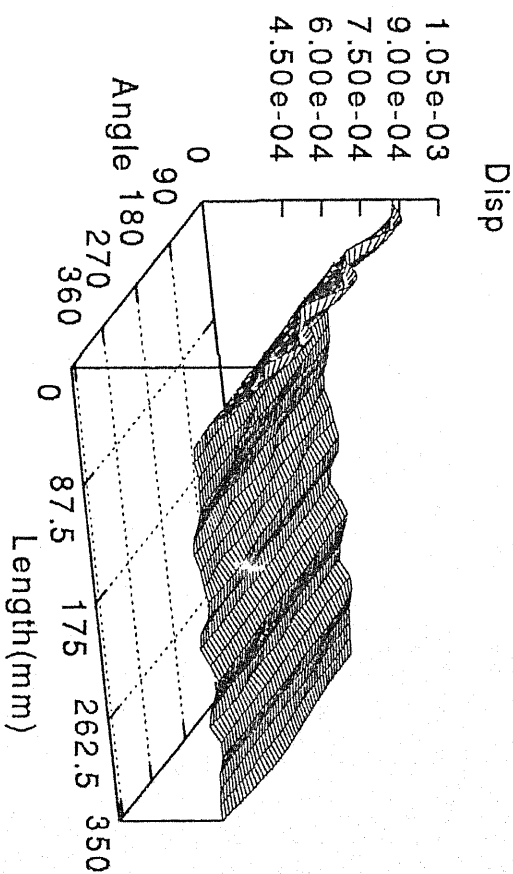
FIG 4.32(cont.): SNAPSHOTS OF AXIAL DISPLACEMENTS

AXIAL CRACK: L=140mm, Θ=120 deg

FIG 4.33: CIRCUMFERENTIAL DISPLACEMENTS AT THREE SOURCE LOCATIONS
AXIAL CRACK: L=140mm, Θ=120 deg
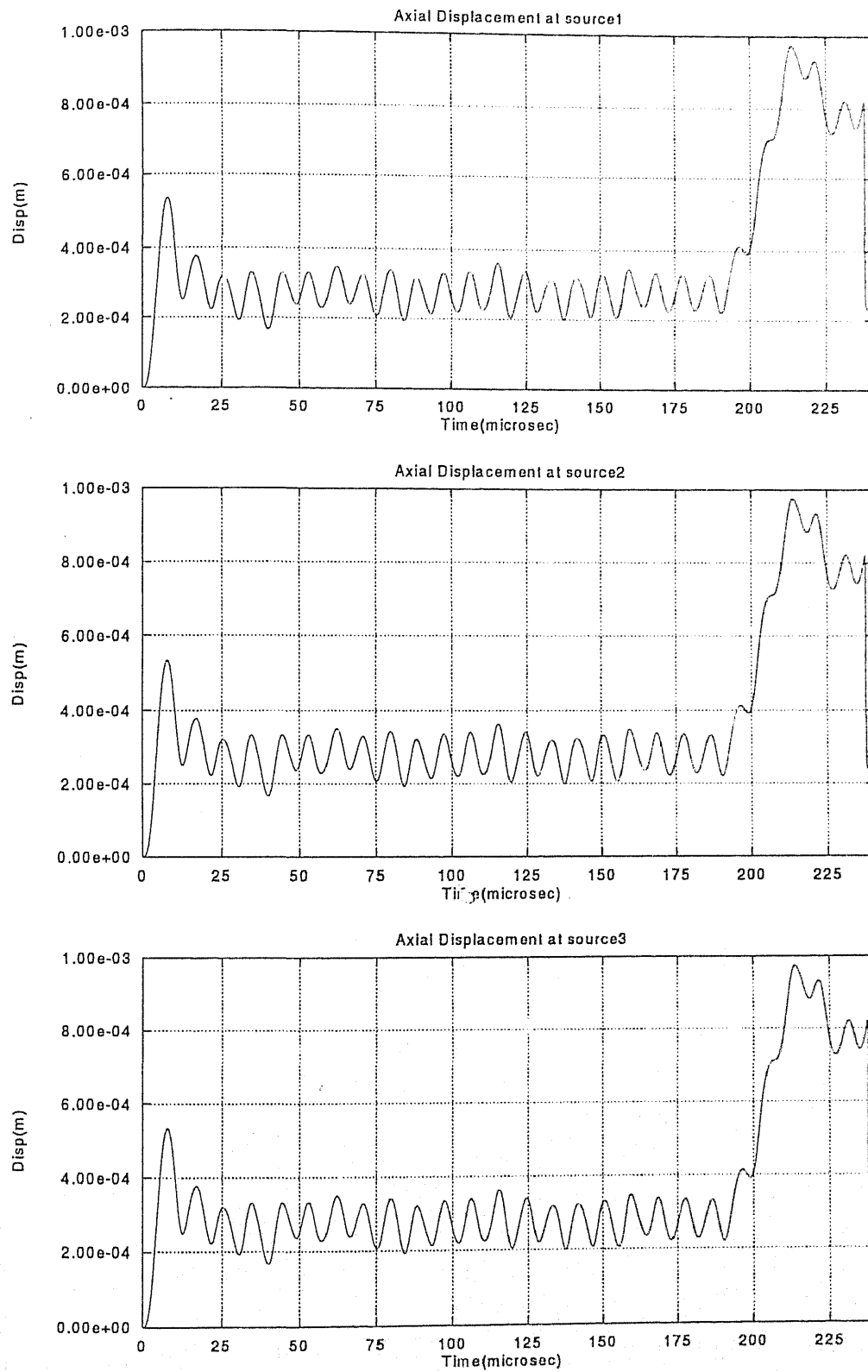
FIG 4.34: AXIAL DISPLACEMENTS AT THREE SOURCE LOCATIONS
AXIAL CRACK: L=140mm, Θ=120 deg
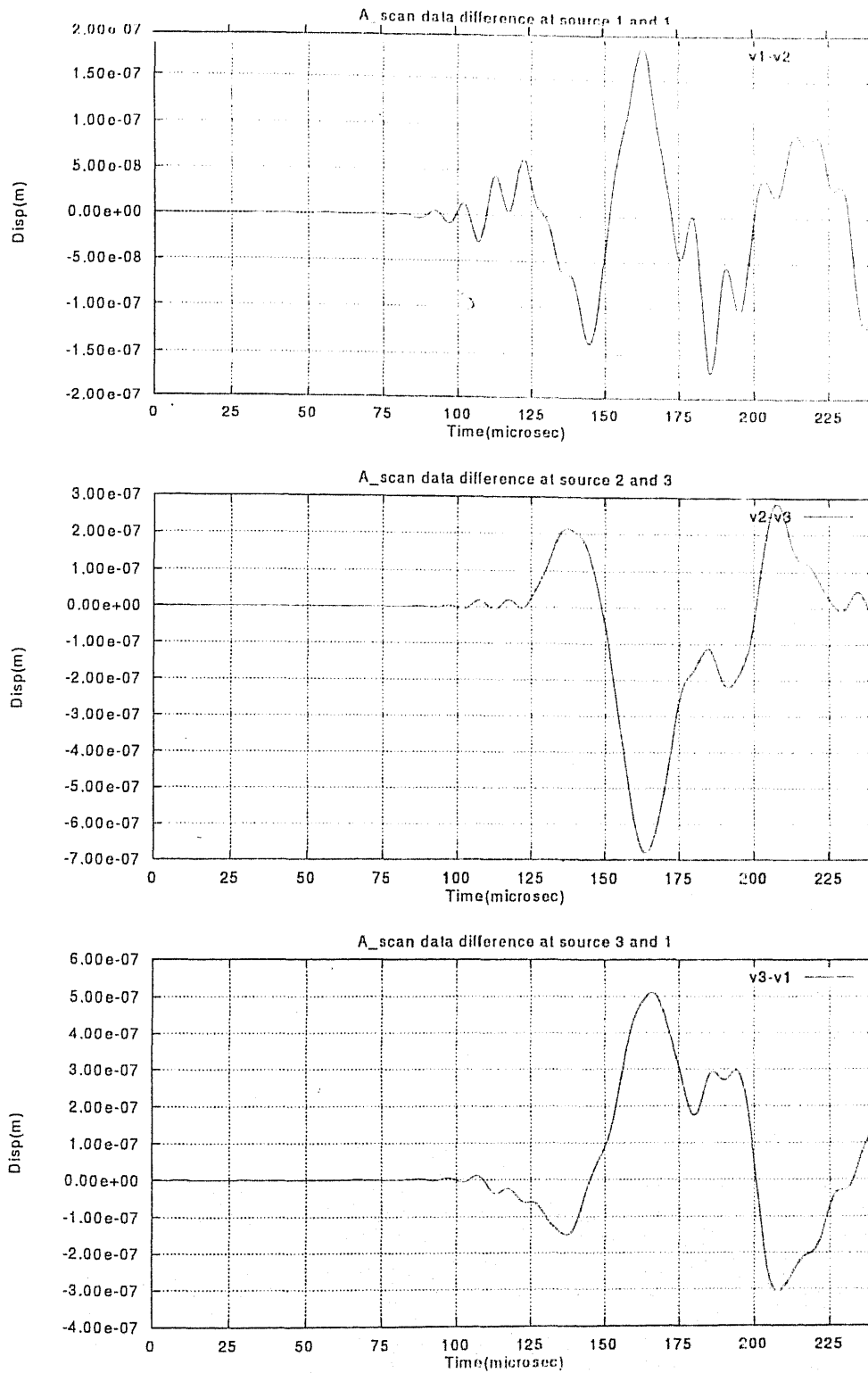
FIG 4.35: A-SCAN PLOTS OF DIFFERENCE OF CIRCUMFERENTIAL DISPLACEMENT
AT THE SOURCE LOCATIONS

CIRCUMFERENTIAL CRACK: L=233.3mm, Θ=225 deg
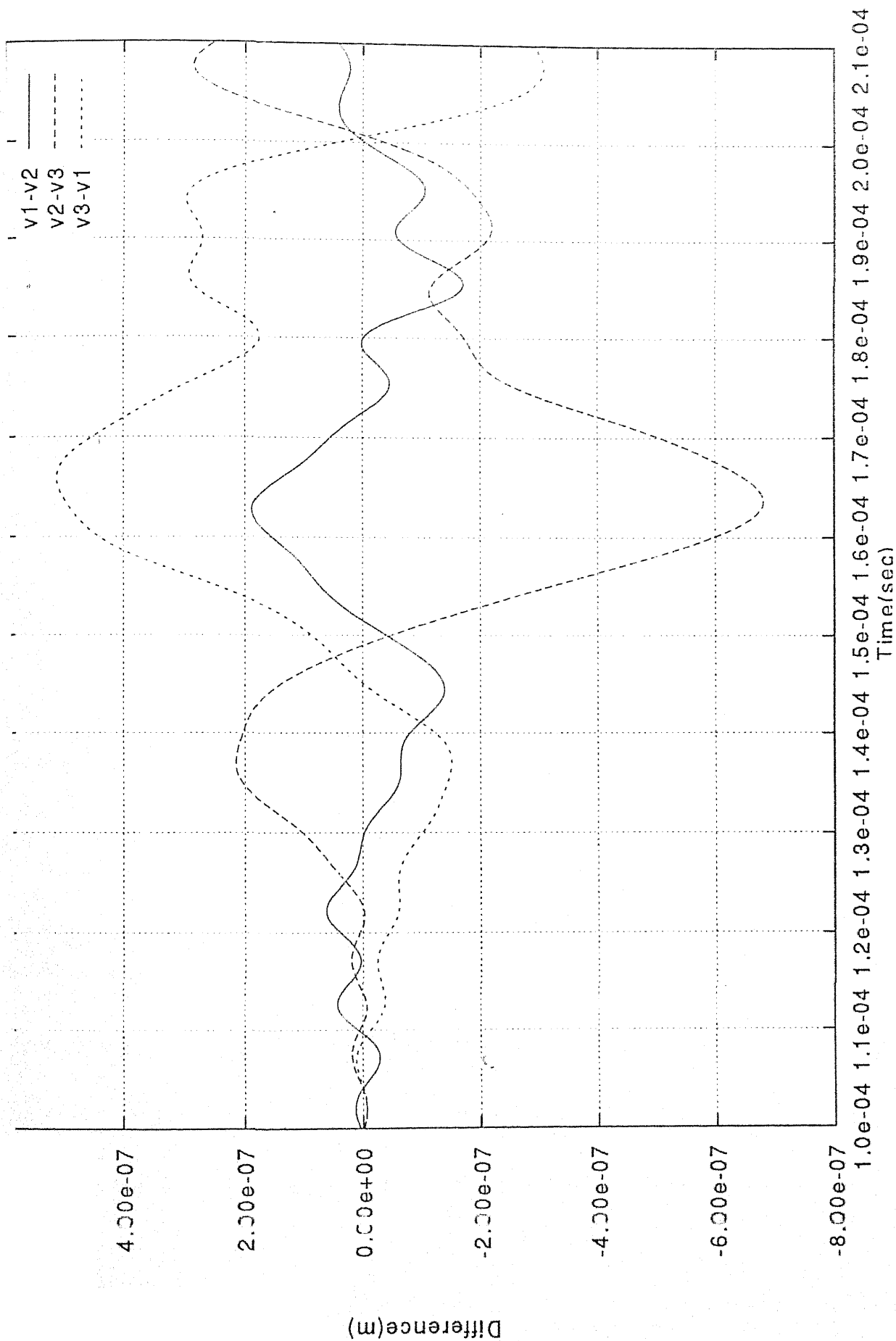
FIG 4.36: A-SCAN PLOTS OF DIFFERENCE OF CIRCUMFERENTIAL DISPLACEMENT AT THE SOURCE LOCATIONS

Chapter 5

Conclusions

5.1 Conclusions

A finite element model has been developed to study the elastic wave propogation and scattering in thin tubes. A number of simulations are performed to suggest a method to determine the axial and angular location of the cracks in thin tubes. The finite element method has been found to be very effective in describing the complex wave/defect interaction.

From the numerical computation point of view it is concluded that the Newmark's time integration scheme along with degenerated shell elements is optimum combination to solve the hyperbolic partial differential equation governing the wave motion in tubes.

From the results of the simulations performed the following conclusions are drawn:

1.A methodology has been suggested to for the detection of location and classification of defects in thin tubes.

2.The method developed helps in clearly locating the axial location of the defect.

3. This method qualitatively gives the angular location of the defect.

4. Using this method long length of the tube can be inspected from each transducer.

5.2 Scope of future work

1.Due to computational restrictions only a small domain was modelled in the present work. Further analysis can be carried out with a finer mesh to get more realistic results.

2.In this work angular location of the crack is found qualitatively, more realistic results can be found by making a quantitative analysis.

3.Transducer models can be incorporated into the code so that the results can be closer to the practical inspection condition.

Bibliography

[1] Pao Y.H 'Elastic Waves in Solids' , J Appl Mechanics, Trans. ASME, Vol. 50, pp 1152-1164, 1983.

[2] Thomson D.O and Chimenti D (editors) 'Review of Progress in Quantitative Nondestructive evaluation', Plenum (newyork), Annual meeting proceedings (1980-92).

[3] Blackmore M and Georgiou G.A (editors) 'Mathematical modelling in NDT', Clarendon press (oxford), 1988.

[4] Datta S.K, Achenbach J.D, Rajapakse .Y.S (editors) 'Elastic Waves and Ultrasonic Nondestructive Evaluation', North-Holland, 1990.

[5] Sharpe R.S (editor) 'Research Techniques in Nondestructive Testing', Academic press, Series (1971-92).

[6] R.H. Gallagher 'Finite Element Analysis: Fundamentals ', Prentice-Hall, 1975.

[7] D.G. Ashwell and R.H. Gallargher (editors) 'Finite Elements for thin shells and curved members', John Wiley and sons, London, 1976.

[8] O.C. Zienkiewicz 'Finite Elament Method', McGraw-Hill Book Company (UK) Limited, 1977.

[9] R.H. Gallagher ' Shell elements, in Proc. of World Congress on Finite Element Methods in Structural Mechanics', Bournemouth, Dorset, England, October 1975. pp. E.1-E.35.

[10] R.H. Gallagher 'Problems and progress in thin shell finite element analysis, in Finite Elements in Thin Shells and Curved Members', D.G. Ashwell and Gallagher (editors), 1976,pp. 1-14.

[11] S. Ahmad, B. M. Irons and O.C. Zienkiewicz 'Analysis of thick and thin shell strustures by curved finite elements', Int. J. Num¿ Meth. Engg., Vol2, 1970, pp. 419-451.

[12] Achenbach J.D, Gautesen A.K and McMaken II (editors) 'Ray Methods for Waves in elastic Solids' Pitman(London).1982.

[13] Olsson P and Bostrom A 'The Null Field and T-matrix Methods for Elastodynamics Scattering problems: cracks and Other Types of Problems' in 'Elastic Waves and Ultrasonic Nondestructive Evaluation' Achenbach J.D (editors),North-Holland, 1990.

[14] Rizzo F.J 'A boundary Integral Equation Method for Radiation and Scattering of Elastic Waves in Three Dimensions', Int. J. Numerical Methods in Eng., Vol. 21 pp 115-129, 1985.

[15] Bond L.J 'Ultrasonic Wave Propagation and Scattering Using Explicit Finite Difference Methods', in 'Mathematical Modelling in NDT' Blackmore M and Georgiou G.A (editors), Clarendon Press (Oxford), pp 61-71, 1986.

[16] Punjani M and Saffari N 'Scattering of Plane Waves by a Partially Closed Crack', in 'Review of Quanditative Nondestructive Evaluation', Thomson D.O and Chimenti D (editors), Plenum (Newyork), Vol. 5A, pp 61-71, 1986.

[17] Bond L.J and Saffari N 'Mode-conversion Ultrsonic Testing', in 'Research Techniques in Nondestructive Testing', Sharpe R.S (editor), Academic Press , Vol. 7,pp 145-189, 1984.

[18] Temple J.A.G 'Modelling The Propagation and Scattering of Elastic waves in Inhomogeneous and Anisotropic Media', J Phys D: Appl Phys., Vol. 21, pp 859-873, 1988.

[19] Kasaburo Harumi 'Comuter Simulation of Ultrasonics in a Solid', Materials Evaluation, Vol. 44,pp 1086-1110, 1986.

[20] Ludwig R and Lord W 'A Finite-element Formulation for the Study of Ultrsonic NDT Systems' IEEE Trans. on Ulttrasonics, Ferroelectrics and Frequency Control, Vol.35, No.6,pp 809-820, 1988.

[21] You Z and Lord W 'Finite Element Study of Elastic Wave Interaction with Cracks', in 'Review of Progress in Quantitative Nondestructive Evaluation' Thomson D.O and Chimenti D.E (editors), Vol. 8A, pp 109-116, Plenum Press, Newyork, 1989.

[22] Seron F.J 'Finite-Element Method for Elastic Wave Propagation' Communications in Applied Numerical Methods, Vol. 6, pp 359-368, 1990.

[34] Ditri, J. J., Rose ,J. L.,and Chen, G.,' MOde Selection Criteria for Defect Detection Optimization Using Lamb Waves,' Review of Progress in Quantitative Nondestructive Evaluation, Vol. 11 , pp. 2109-2115, 1992b.

[35] Rose, J. L., Ditri, J.J., Pilarski, A., Rajana, K. M. and Carr, F.'A guided wave Inspection Tecnique for Nuclear Steam Generator Tubing,' NDT&E International, Vol 27, No 6, pp. 307-310, 1993.

[36] Rose, J. L., Rajana, K. M. and Carr, F.T .,' Ultrasonic Guided Wave Inspection Concepts for Steam Generator Tubing', Materials Evaluation, Vol. 13, 1994, pp.307-311.

[37] Rose, J. L., Cho, Y and Ditri, J.J., 'Cylidrical Guided Wave Leakage Due to Liquid Loading,' Review of Progress in Quantitative Nondestructive Evaluation, Vol. 13, 1994. pp. 259-266.

[38] Alleyne, and Cawley, P., ' The Intersection of Lamb Waves with defects,' IEEE Transactions on Ultrasonics, Ferroelectrics, and Frequency Control, Vol. 39 No. 3 , pp. 381-397, 1992.

[39] Ditri, J. J. ' Utilization of guided elastic waves for characterization of circumferential cracks in hollow cylinders,' J. Acoust. Soc. Am., Vol. 96 3769-3775 1994.

[40] Ditri, J. J and Rose, J. L., 'Excitation of guided waves modes in hollow cylinders by applied surface tractions,' J. Acoust. Soc. Am., Vol. 72 2589-2597, 1992.

A 125484

ME- 1998 - M - KAN - FIN